Message-Passing on Hypergraphs: Detectability, Phase Transitions and Higher-Order Information

Nicolò Ruggeri,[1,2,*] Alessandro Lonardi,[1,†] Caterina De Bacco[1,‡]

[1]*Max Planck Institute for Intelligent Systems, Cyber Valley, Tübingen 72076, Germany*
[2]*Department of Computer Science, ETH, Zürich 8004, Switzerland*

Hypergraphs are widely adopted tools to examine systems with higher-order interactions. Despite recent advancements in methods for community detection in these systems, we still lack a theoretical analysis of their detectability limits. Here, we derive closed-form bounds for community detection in hypergraphs. Using a Message-Passing formulation, we demonstrate that detectability depends on hypergraphs' structural properties, such as the distribution of hyperedge sizes or their assortativity. Our formulation enables a characterization of the entropy of a hypergraph in relation to that of its clique expansion, showing that community detection is enhanced when hyperedges highly overlap on pairs of nodes. We develop an efficient Message-Passing algorithm to learn communities and model parameters on large systems. Additionally, we devise an exact sampling routine to generate synthetic data from our probabilistic model. With these methods, we numerically investigate the boundaries of community detection in synthetic datasets, and extract communities from real systems. Our results extend the understanding of the limits of community detection in hypergraphs and introduce flexible mathematical tools to study systems with higher-order interactions.

I. INTRODUCTION

Modeling complex systems as graphs has broadened our understanding of the macroscopic features that emerge from the interaction of individual units. Among the various aspects of this problem, community detection stands out as a fundamental task, as it provides a coarse-grained description of a network's structural organization. Notably, community structure is observed across different systems, such as food webs [1], spatial migration and gene flow of animal species [2], as well as in social networks [3], power grids [4], and others [5].

In the case of networks with only pairwise interactions, there are solid theoretical results on detectability limits, describing whether the task of community detection can or cannot succeed [6–11]. However, many complex systems with interactions that extend beyond pairs are better modeled by hypergraphs [12], which generalize the simpler case of dyadic graphs. Phenomena that have been investigated on graphs are now readily explored on hypergraphs, with examples including diffusion processes, synchronization, phase transitions [13] and, more recently, community structure [14–18].

Extending the rigorous results of detectability transitions for networks to higher-order interactions is a relevant open question.

One of the main obstacles in modeling hypergraphs is their intrinsic complexity, which poses both theoretical and computational challenges and restricts the range of results available in the literature. The difficulty of defining communities in hypergraphs and of deriving theoretical thresholds for their recovery has limited investigations to the study of d-uniform hypergraphs, i.e., hypergraphs that only contain interactions among exactly d nodes [19–27].

A related line of literature focuses on the detection of planted sub-hypergraphs [28, 29] and testing for the presence of community structure in hypergraphs [30, 31]. Generally, extracting

recovery results on non-uniform hypergraphs proved to be demanding, with scarce literature on the subject.

Recently, Chodrow *et al.* [32] conjectured a recoverability threshold for their spectral clustering algorithm on non-uniform hypergraphs. Closer to the scope of our work, Dumitriu and Wang [18] provide a probabilistic model and bounds for the theoretical recovery of communities under the same model. However, such detectability bounds are based on algorithms which are not feasible in practice, and no empirical demonstration of the predicted recovery is provided. Furthermore, all these methods lack a variety of desirable probabilistic features, such as the estimation of marginal probabilities of a node to belong to a community, a principled procedure to sample synthetic hypergraphs with prescribed community structure, and the possibility to investigate the energy landscape of a problem via free energy estimations.

In this work, we address these issues by deriving a precise detectability threshold for hypergraphs that depends on the node degree distribution, the assortativity of the hyperedges, and crucially, on higher-order properties such as the distribution of hyperedge sizes. Additionally, we show how these properties can be formally described via notions of entropy and information, leading to a clear interpretation of the role of higher-order interaction in detectability.

Our approach is based on a probabilistic generative model and a related Bayesian inference procedure, which we utilize to study the limits of the community detection problem using a Message-Passing (MP) formulation [33–35], originating from the cavity method in statistical physics [36, 37]. We focus on an extension to hypergraphs of the stochastic block model (SBM) [38, 39], a generative model for networks with community structure. Several variants of the SBM [15], and of its mixed-membership version [16, 17], have been extended to hypergraphs. The model we utilize is an extension of the dyadic SBM to hypergraphs and allows generalizing the seminal detectability results of Decelle *et al.* [6, 7] to higher-order interactions.

In addition to our theoretical contributions, we derive an algorithmic implementation for inferring both communities and parameters of the models from the data. Our implementation

scales well to both large hypergraphs and large hyperedges, owing to a dynamic-program formulation.

Finally, we show how, with additional combinatorial arguments, one can efficiently sample hypergraphs with arbitrary communities from our probabilistic model. This problem, often studied in conjunction with inference, deserves its own attention when dealing with hypergraphs, as recently discussed in related work [40, 41].

Through numerical experiments, we confirm our theoretical calculations by showing that our algorithm accurately recovers the true community structure in synthetic hypergraphs all the way down to the predicted detectability threshold. We also illustrate that our approach gives insights into the community organization of real hypegraphs by analyzing a dataset of group interactions between students in a school. To facilitate reproducibility, we release open source the code that implements our inference and sampling procedures [42].

II. THE HYPERGRAPH STOCHASTIC BLOCK MODEL

Consider a hypergraph $H = (V, E)$ where $V = \{1, ..., N\}$ is the set of nodes and E the set of hyperedges. A hyperedge e is a set of two or more nodes. We define $\Omega = \{e : 2 \leq |e| \leq D\}$, the set of all possible hyperedges up to some maximum dimension $D \leq N$, with $|e|$ being the size of a hyperedge, i.e., the number of nodes it contains. Notice that $E \subseteq \Omega$. We denote with $A_e = 1$ all $e \in E$ and with $A_e = 0$ hyperedges $e \in \Omega \setminus E$.

Our Hypergraph Stochastic Block Model (HySBM) is an extension of the classical SBM for graphs [38, 39]. It partitions nodes into K communities by assigning a hard membership $t_i \in [K] \equiv \{1, \ldots, K\}$ to each node $i \in V$. It does so probabilistically, assuming that the likelihood to observe a hyperedge A_e is a Bernoulli distribution with a parameter that depends on the memberships $\{t_i\}_{i \in e}$ of its nodes. Formally, the probabilistic model is summarized as

$$t_i \sim \mathrm{Cat}(n) \qquad \forall i \in V \tag{1}$$

$$A_e \,|\, t \sim \mathrm{Be}\left(\frac{\pi_e}{\kappa_{|e|}}\right) \quad \forall e \in \Omega\,, \tag{2}$$

where $n = (n_1, \ldots, n_K)$ is a vector of prior categorical probabilities for the hard assignments t_i. The Bernoulli probabilities are given by

$$\pi_e = \sum_{i < j \in e} p_{t_i t_j}\,, \tag{3}$$

with $0 \leq p_{ab} \leq 1$ being elements of a symmetric probability matrix (also referred to as affinity matrix) and $\kappa_{|e|}$ a normalizing constant that only depends on the hyperedge size $|e|$. This can take on any values, provided that it yields sparse hypergraphs where $\pi_e/\kappa_{|e|} = O(1/N)$ and valid probabilities $\pi_e/\kappa_{|e|}$. We develop our theory for a general form of $\kappa_{|e|}$ and elaborate more on its choice in Appendix A. In our experiments we utilize the value $\kappa_d = \binom{N-2}{d-2}\frac{d(d-1)}{2}$ [17, 41].

Our specific formulation of the likelihood is only one among many alternatives to model communities in hypergraphs. The

likelihood we propose has three main properties. First, HySBM reduces to the standard SBM when only pairs are present (as $\kappa_2 = 1$). Since we aim to develop a model that generalizes the SBM to hypergraphs, this is an important condition to satisfy. Second, it enables to develop the MP equations presented in the following section, which in turn lead to a theoretical characterization of the detectability limits and a computationally efficient algorithmic implementation. Third, the likelihoods based on expressions similar to Eq. (3) have been shown to well describe higher-order interactions that possibly contain nodes from different communities [41].

For convenience, we work with a rescaled affinity matrix $c = Np$, which is of order $c = O(1)$ in sparse hypergraphs. The log-likelihood $\mathcal{L} \equiv \mathcal{L}(A, t \,|\, p, n)$ evaluates to

$$
\begin{aligned}
\mathcal{L} &= \sum_{e \in \Omega} \left[A_e \log\left(\frac{\pi_e}{\kappa_e}\right) + (1 - A_e) \log\left(1 - \frac{\pi_e}{\kappa_e}\right) \right] \\
&\quad + \sum_{i \in V} \log n_{t_i} \\
&= \sum_{e \in \Omega} \left[A_e \log\left(\sum_{i < j \in e} c_{t_i t_j} \right) + (1 - A_e) \right. \\
&\quad \left. \times \log\left(1 - \frac{\sum_{i < j \in e} c_{t_i t_j}}{N \kappa_e} \right) \right] + \sum_{i \in V} \log n_{t_i} + \mathrm{const.}\,,
\end{aligned}
\tag{4}
$$

where $\mathrm{const.}$ denotes quantities that do not depend on the parameters of the model.

III. INFERENCE AND GENERATIVE MODELING

A. Induced factor graph representation

The probabilistic model in Eqs. (1)–(2) has a negative log-likelihood that can be interpreted as the Hamiltonian of a Gibbs-Boltzmann distribution on the community assignments t:

$$p(t \,|\, A, p, n) = \frac{p(A, t \,|\, p, n)}{p(A \,|\, p, n)} = \frac{\exp \mathcal{L}(A, t \,|\, p, n)}{Z}\,, \tag{5}$$

where Z is the partition function of the system, that corresponds to the marginal likelihood of the data. The quantity $F = -\log Z$ is also called the free energy. The equivalence in Eq. (5) allows interpreting the probabilistic model in terms of factor graphs [34]. Here, the function nodes are hyperedges $f \in \Omega$, and variable nodes are elements of V. The interactions between function and variable nodes can be read directly from the log-likelihood in Eq. (4). In other words, the probabilistic model induces a factor graph $F = (\mathcal{V}, \mathcal{F}, \mathcal{E})$ with variable nodes $\mathcal{V} = V$, function nodes $\mathcal{F} = \Omega$ and edges $\mathcal{E} = \{(i, e) \in \mathcal{V} \times \mathcal{F} : i \in e\}$. In Fig. 1 we show a graphical representation of the equivalence between hypergraphs and factor graphs. For any variable node i and function node f of the factor graph we define the neighbors, or boundaries, as $\partial i = \{f \in \mathcal{F} : (i, e) \in \mathcal{E}\}$, being all function nodes adjacent to i, and $\partial f = \{i \in \mathcal{V} : (i, e) \in \mathcal{E}\}$ being all variable nodes adjacent to f.
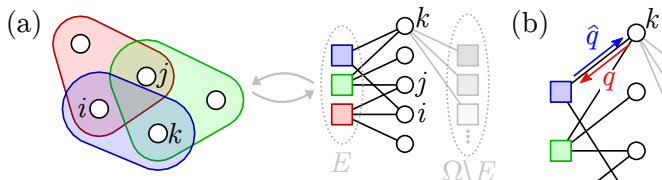
FIG. 1: **Representing hypergraphs as factor graphs. (a)** We depict a hypergraph and its factor graph equivalent. In the factor graph $\mathcal{F}$, function nodes represent hyperedges. Notice that, while the node sets are the same in both representations, due to the presence of all possible hyperedges in the log-likelihood in Eq. (4), the factor graph does not only contain the observed interactions E (black), but also the unobserved ones $\Omega \setminus E$ (gray). **(b)** In factor graphs, there are two types of messages: variable-to-function node q (red), and function-to-variable node $\hat{q}$ (blue).

B. Message-Passing (MP)

Given the factor graph representation of HySBM, we can perform Bayesian inference of the community assignments via message-passing. Originally obtained from the cavity method on spin glasses [36, 37], MP allows estimating marginal distributions on the variable nodes of a graphical model by iteratively updating messages, auxiliary variables that operate on the edges of the factor graph. The efficiency of MP comes from the fact that the structure of the factor graph favors locally distributed updates. Although exact theoretical results are only proven on trees, MP has been shown to obtain strong performance also on locally tree-like graphs [34] and it has been extended to dense graphs with short loops [43, 44].

Applying MP to our model, the inference procedure yields expressions for the marginal probabilities $q_i(a)$ of a node i to be assigned to any given community $a \in [K]$. Their values are obtained as solutions to closed-form fixed-point equations, which involve messages $q_{i \to e}(t_i)$ from variable to function nodes, and $\hat{q}_{e \to i}(t_i)$, from function to variable nodes. The messages follow the sum-product updates

$$q_{i \to e}(t_i) \propto n_{t_i} \prod_{f \in \partial i \setminus e} \hat{q}_{f \to i}(t_i) \tag{6}$$

$$\hat{q}_{e \to i}(t_i) \propto \sum_{t_j : j \in \partial e \setminus i} \left(\frac{\pi_e}{\kappa_e}\right)^{A_e} \left(1 - \frac{\pi_e}{\kappa_e}\right)^{1-A_e} \prod_{j \in \partial e \setminus i} q_{j \to e}(t_j), \tag{7}$$

and yield marginal distributions as

$$q_i(t_i) \propto n_{t_i} \prod_{e \in \partial i} \hat{q}_{e \to i}(t_i). \tag{8}$$

Notice that, compared to those for graphs, the MP equations for hypergraphs in Eqs. (6)–(8) present additional challenges. First, in graphs the updates simplify. One can in fact collapse the two types of messages (and equations) into a unique one, since paths (i, f, j) in the factor graph reduce to pairwise interactions (i, j) between nodes. This simplification is not possible in hypergraphs, as one function node may connect more

than two variable nodes. Second, the dimensionality of the MP equations grows faster when accounting for higher-order interactions. Here, the number of function nodes is equal to $|\mathcal{F}| = |\Omega| = \sum_{d=2}^{D} \binom{N}{d}$, yielding $|\mathcal{F}| = O(2^N)$ at large $D = N$. In contrast, one gets $O(N^2)$ pairwise messages in the updates for graphs. To produce computationally feasible MP updates one can assume sparsity, as already done in the dyadic case. We outline such updates in the following theorem.

Theorem 1. *Assuming sparse hypergraphs where $c = O(1)$, the MP updates satisfy the following fixed-point equations to leading order in N. For all hyperedges $e \in E$ and nodes $i \in e$, the messages and marginals are given by:*

$$q_{i \to e}(t_i) \propto n_{t_i} \left(\prod_{\substack{f \in E \\ f \in \partial i \setminus e}} \hat{q}_{f \to i}(t_i) \right) \exp(-h(t_i)) \tag{9}$$

$$\hat{q}_{e \to i}(t_i) \propto \sum_{t_j : j \in \partial e \setminus i} \pi_e \prod_{j \in \partial e \setminus i} q_{j \to e}(t_j) \tag{10}$$

$$q_i(t_i) \propto n_{t_i} \left(\prod_{\substack{f \in E \\ f \in \partial i}} \hat{q}_{f \to i}(t_i) \right) \exp(-h(t_i)) \tag{11}$$

$$h(t_i) = \frac{C'}{N} \sum_{j \in V} \sum_{t_j} c_{t_i t_j} q_j(t_j), \tag{12}$$

where $C' = \sum_{d=2}^{D} \binom{N-2}{d-2} \frac{1}{\kappa_d}$.

A proof of Theorem 1 is provided in Appendix B. The updates in Eqs. (9)–(12) are in principle computationally feasible, as products of function nodes $f \in E$ have replaced products over the entire space $f \in \Omega$. In sparse graphs, that we observe in many real datasets, E is much smaller than the original Ω, thus significantly decreasing the computation cost. An intuitive justification of Theorem 1, which we formalize in its proof, is that the observed interactions $f \in E$ hold most of the weight in the updates of their neighbors, while the unobserved ones $f \in \Omega \setminus E$ send approximately constant messages and thus can be absorbed in the external field h introduced in Eq. (12). This idea is inspired by the dyadic MP equations in Decelle *et al.* [6]. However, in contrast to MP on graphs, a vanilla implementation of the updates is still not scalable in hypergraphs, as the computational cost of Eq. (10) is $O(K^{|e|-1})$. To tackle this issue, we develop a dynamic programming approach that reduces the complexity to $O(K^2|e|)$. Dynamic programming is exact, as it does not rely on further approximations on the MP updates, its detailed derivations are provided in Appendix D 1.

The fixed-point equations of Theorem 1 naturally suggest an algorithmic implementation of the MP inference procedure. We present a pseudocode for it in Appendix D 2.

C. Expectation-Maximization to learn the model parameters

We have presented a MP routine for inferring the community assignments $\{t_i\}_{i \in V}$. Now, we derive closed-form updates for the model parameters c, n via an Expectation-Maximization

(EM) routine [45]. Differentiating the log-likelihood in Eq. (4) with respect to n, and imposing the constraint $\sum_{a=1}^{K} n_a = 1$, yields the update

$$n_a = \frac{N_a}{N} \, . \tag{13}$$

Notice that this update depends on the MP results, as $N_a = |\{i \in V : \arg\max_b q_i(b) = a\}|$ is the count of nodes assigned to community a according to the inferred marginals. To update the rescaled affinity c we adopt a variational approach, where we maximize a lower bound of the log-likelihood, or, equivalently, minimize a variational free energy. In Appendix C, we show detailed derivations for the following fixed-point updates

$$c_{ab}^{(t+1)} = c_{ab}^{(t)} \frac{2 \sum_{e \in E} \#_{ab}^e / \pi_e}{N \, C' \, (N n_a n_b - \delta_{ab} n_a)} \, , \tag{14}$$

where $\#_{ab}^e = \sum_{i < j \in e} \delta_{t_i a} \delta_{t_j b}$ is the count of dyadic interactions between two communities a, b within a hyperedge e. In practice, when inferring t, n, c one proceeds by alternating MP inference of t, as presented in Sec. III B, with the updates of c and n in Eqs. (13)–(14) until convergence. A pseudocode for the EM procedure is presented in Appendix D 2.

D. Sampling from the generative model

One of the main advantages of using a probabilistic formulation, such as the one presented here, is the ability to generate data with a desired community structure. Among other tasks, this can be used in particular to test detectability results like the ones we theoretically derive in the following section. However, in hypergraphs, writing a probabilistic model does not directly imply the ability to sample from it, as is typically the case for graphs [40, 41]. In fact, while the $O(N^2)$ configuration space of graphs allows performing sampling explicitly, in the case of hypergraphs the exploding configuration space Ω makes this task prohibitive, even for hypergraphs with moderate number of nodes and hyperedge sizes. Here we propose a novel sampling algorithm that can efficiently scale and produce hypergraphs of dimensions in the tens or hundreds of thousands of nodes. We exploit the hard-membership nature of the assignments to obtain exact sampling via combinatorial arguments, as opposed to the approximate sampling in recent work for mixed-membership models [41]. Owing to this procedure, our results are not limited to theoretical derivations, but can be tested numerically on synthetic data, as we show below. Hence, our sampling routine is an essential contribution of this work. The details of our sampling procedure are presented in Appendix E and its implementation is open sourced [42].

IV. PHASE TRANSITION

A. Detectability bounds

Beside providing a valid and efficient inference algorithm, one of the main advantages of MP is the possibility of deriving closed-form expressions for the detectability of planted communities. The transition from detectable to undetectable regimes has been first shown to exist in MP-based inference models for graphs [6], and gave rise to an extensive body of literature on theoretical detectability limits and sharp phase transitions [8, 9]. Here, we extend these classical arguments to hypergraphs, and find relevant differences when higher-order interactions are considered.

In line with previous work, we restrict our study to the case where groups have constant expected degrees. In fact, in settings where such an assumption does not hold, it is possible to obtain good classification by simply clustering nodes based on their degrees [6]. Formally, we assume

$$\sum_{a=1}^{K} c_{ab} n_b = c \, , \tag{15}$$

for some fixed constant c. Notice that Eq. (15) does not immediately imply a constant degree for the groups, as in hypergraphs the expected degree is defined differently than the left-hand-side of the equation above. Nevertheless, in Appendix F 1 we prove that imposing the condition in Eq. (15) does indeed imply a constant average degree. More precisely,

Proposition 1. *Assuming Eq.* (15)*, the following holds:*

- *all the groups have the same expected degree;*

- *the fixed points for the messages read*

$$q_{i \to e}(t_i) = n_{t_i} \quad \forall e \in E, i \in e \tag{16}$$

$$\widehat{q}_{e \to i}(t_i) = \frac{1}{K} \quad \forall e \in E, i \in e \, . \tag{17}$$

We want to study the propagation of perturbations around the fixed points of Eqs. (16)–(17). We assume that the factor graph is locally tree-like, i.e., neighborhoods of nodes are approximately trees. We provide a visualization of this in Fig. 2. Classically, it has been proven that for sparse graphs almost all nodes have local tree-like structures up to distances of order $O(\log N)$ [34]. We are not aware of similar statements for hypergraphs. While our empirical results prove that these assumptions are reasonable and approximately valid, we leave the formalization of such an argument for future work.

Referring to Fig. 2(b), one can see that between every leaf and the root, there is a single connecting path. Thus, perturbations on the leaves propagate through a tree to the root, and transmit via the following transition matrix

$$\tilde{T}_r^{ab} = \frac{\partial q_{i_r \to f_r}(a)}{\partial q_{i_{r+1} \to f_{r+1}}(b)} \, , \tag{18}$$

where i_r, f_r are respectively the r-th variable node and function node in the path. In words, this is the dependency of a message on the message one level below in the path. In Appendix F 2 we show that, to leading terms in N, the transition matrix evaluates to

$$\tilde{T}_r^{ab} = \frac{2 \, n_a}{|f_r|(|f_r|-1)} \left(\frac{c_{ab}}{c} - 1 \right) \, . \tag{19}$$
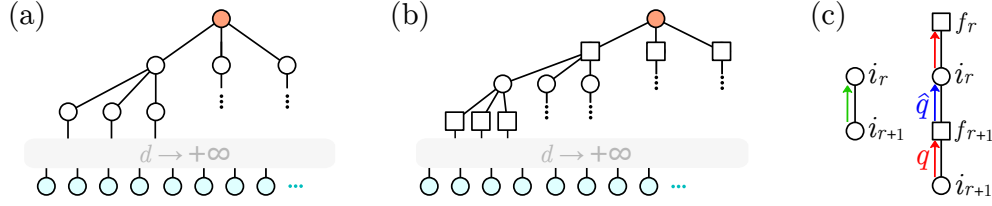
FIG. 2: **Local tree assumption.** **(a)** The classical local tree assumption for graphs. Here, it is assumed that the neighborhoods of nodes are approximately trees. **(b)** The tree assumption for factor graphs. Here, a path from a leaf (light blue) to a root (orange) consists of steps alternating variable nodes and function nodes. These two representations coincide in the case of graphs. **(c)** The perturbations propagate up the tree via the messages. In graphs (a), they reach the root passing from nodes i_{r+1} to i_r (green). In hypergraph-induced factor graphs, perturbations spread from a node i_{r+1}, at depth $r+1$, to its neighboring function nodes f_{r+1} (red), and up to node i_r at depth r (blue) in an alternating fashion.

A related expression was previously obtained for the transition matrix on graphs is $T^{ab} = n_a(c_{ab}/c - 1)$ [6]. Hence, we can compactly write $\tilde{T}_i^{ab} = [2/(|f_r|(|f_r|-1))]\,T^{ab}$. This connection highlights an important difference between the two cases: hyperedges induce a higher-order prefactor with a "dispersion" effect. The larger the hyperedge, the lower is the magnitude of this transition. Instead, if the hyperedge is a pair, this prefactor reduces to one, and we recover the result on graphs. A perturbation $\epsilon_{t_d}^{k_d}$ of a leaf node k_d influences the perturbation $\epsilon_{t_0}^{k_0}$ on the root t_0 by

$$\epsilon_{t_0}^{k_0} = \sum_{\{t_r\}_{r=1,\dots,d}} \left(\prod_{r=0}^{d-1} \tilde{T}_i^{t_r t_{r+1}} \right) \epsilon_{t_d}^{k_d} \,. \tag{20}$$

We can also express this connection in matrix form as

$$\epsilon^{k_0} = \left(\prod_{r=0}^{d-1} \frac{2}{|f_r|(|f_r|-1)} \right) T^d \epsilon^{k_d} \,, \tag{21}$$

where T is the matrix with entries T^{ab} (in Eq. (21) raised to the power of d), and ϵ^{k_d} the array of $\epsilon_{t_d}^{k_d}$ values. Now, similarly to Decelle *et al.* [6], we consider paths of length $d \to +\infty$. In such a case, the r-dependent prefactor in Eq. (21) converges almost surely to

$$\mu = \exp\left(\mathbb{E}\left[d \log \frac{2}{|f|(|f|-1)} \right] \right) \,, \tag{22}$$

where the expectation is taken with respect to randomly drawn hyperedges $f \in E$. If λ is the leading eigenvector of T, then

$$\epsilon^{k_0} \approx \mu\, \lambda^d \epsilon^{k_d} \,. \tag{23}$$

Aggregating over the leaves, and since the perturbations have an expected value of zero, we obtain variance:

$$\langle (\epsilon_{t_0}^{k_0})^2 \rangle \approx \left\langle \left(\frac{[\langle d \rangle (F-1)]^d}{\sum_{k=1}} \mu\, \lambda^d \epsilon_t^k \right)^2 \right\rangle \tag{24}$$

$$\overset{\text{i.i.d.}}{=} (\langle d \rangle (F-1))^d \mu^2 \lambda^{2d} \langle (\epsilon_t^k)^2 \rangle \,, \tag{25}$$

where $\langle d \rangle$ is the average node degree and F the average hyperedge size. The expression in Eq. (25) yields the following stability criterion, the key result of our derivations:

$$\langle d \rangle (F-1) \left(\exp \mathbb{E}\left[\log \frac{2}{|f|(|f|-1)} \right] \right)^2 \lambda^2 < 1 \,. \tag{26}$$

This generalizes the seminal result $c\lambda^2 < 1$ of Decelle *et al.* [6] to hypergraphs. When Eq. (26) holds, the influence of the leaves to the root decays when propagating up the tree in Fig. 2(b). Conversely, if Eq. (26) is not satisfied, it grows exponentially.

To obtain more interpretable bounds, we focus on a benchmark scenario where the affinity matrix contains all equal on- and off-diagonal elements, i.e., $c_{aa} = c_{\text{in}}$ for all $a \in [K]$ and $c_{ab} = c_{\text{out}}$ for all $a \neq b$. In this case, condition Eq. (15) becomes $c_{\text{in}} + (K-1)c_{\text{out}} = Kc$, the leading eigenvalue of T is $\lambda = (c_{\text{in}} - c_{\text{out}})/Kc$, and the stability condition in Eq. (26) reads

$$|c_{\text{in}} - c_{\text{out}}| > \frac{Kc}{\sqrt{\langle d \rangle (F-1)}} \exp\left(-\mathbb{E}\left[\log \frac{2}{|f|(|f|-1)} \right] \right) \,. \tag{27}$$

When hypergraphs only contain dyadic interactions, Eq. (27) reduces to the bound $|c_{\text{in}} - c_{\text{out}}| > K\sqrt{c}$ previously derived for graphs [6], also known as Kesten-Stigum bound [46, 47].

B. Phase transition in hypergraphs

We test the bound obtained in Eq. (27) by running MP on synthetic hypergraphs generated via the sampling algorithm of Sec. III D. In our experiments, we fix $K = 4$ and sample hypergraphs with $N = 10^4$ nodes. We also fix $c = 10$ and change the ratio $c_{\text{out}}/c_{\text{in}}$. In this setup, for graphs, one expects a continuous phase transition between two regimes where the system is undetectable and detectable [6]. In the former, where the inequality yielded by the Kesten-Stigum bound does not hold, and the graph does not carry sufficient information about the community assignments, community detection is impossible. In the latter, communities can be efficiently recovered by MP. In Fig. 3 we plot the overlap $= (\sum_i q_i^\star/N - \max_a n_a)/(1 - \max_a n_a)$ with $q_i^\star \equiv q_i(a_i^\star)$ and
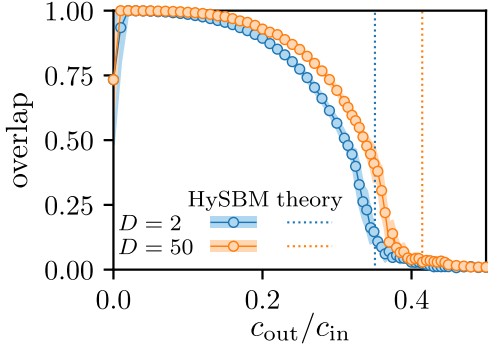
FIG. 3: **Phase transition.** The overlap between ground truth and inferred communities varies for different $c_{\mathrm{out}}/c_{\mathrm{in}}$ ratios. The values attained are positive on the detectable region (left of the dotted theoretical bounds) and continuously drop to zero as the phase transition boundary approaches. Values for hyperedges up to size $D = 50$ (orange) always yield higher overlap compared to $D = 2$ (light blue). Shaded areas are standard deviations over 5 random initializations of MP.

$a_i^\star = \arg\max_b q_i(b)$, against $c_{\mathrm{out}}/c_{\mathrm{in}}$. Our results are in agreement with the theoretical predictions: the overlap is low in the undetectable region, high in the detectable region, and we observe a continuous phase transition at the Kesten-Stigum bound for graphs, i.e., when $D = 2$.

We expect the presence of higher-order interactions to improve detectability, as it yields greater overlap for any $c_{\mathrm{out}}/c_{\mathrm{in}}$ and it shifts the theoretical transition to larger values. We empirically validate this prediction by evaluating Eq. (27) for hyperedges up to size $D = 50$ and performing MP inference in Fig. 3. Diverging convergence times for larger $c_{\mathrm{out}}/c_{\mathrm{in}}$, i.e., when the free energy landscape gets progressively rugged, further demonstrate this behavior, as shown in Appendix F 3.

C. The impact of higher-order interactions on detectability

As mentioned above, the transition matrix in Eq. (19) reduces to the classic T^{ab} [6] when only dyadic interactions are present. In fact, the additional prefactor $2/(|f_r|(|f_r|-1))$ is equal to one for 2-dimensional hyperedges. However, when hyperedges of higher sizes are present, this prefactor is strictly smaller than one. This dampens the perturbations ϵ^{k_0} when they propagate up the tree in Fig. 2(b). It is unclear whether this higher-order effect aids or hurts detectability, as it could prevent signal from being propagated, but also noise from accumulating at the root.

With this in mind, we investigate the impact of higher-oder interactions on detectability by disentangling the effect that K, c and, most importantly, D have on the detectability bound set by Eq. (26). To this end, we rewrite Eq. (27) as

$$\left| \rho_{\mathrm{in}} - \frac{1}{Kc} \right| > \Phi(K, c, D). \tag{28}$$

Here, we utilized $c_{\mathrm{in}}/Kc = \rho_{\mathrm{in}} \in [0, 1]$, a degree-independent rescaling of c_{in}, where we normalize by its maximum possible

value Kc, as per Eq. (15). The term $\Phi(K, c, D)$ is the value of the theoretical bound at the r.h.s. of Eq. (27), normalized by Kc as well. This way, we get the decomposition $\Phi(K, c, D) = \alpha(K)\beta(c)\gamma(D)$ as a product of three independent terms:

$$\alpha(K) = \frac{K - 1}{K} \tag{29}$$

$$\beta(c) = \frac{1}{\sqrt{c}} \tag{30}$$

$$\gamma(D) = \frac{\exp\left(-\mathbb{E}\left[\log \frac{2}{|f|(|f|-1)}\right]\right)}{\sqrt{C(F-1)/2}}, \tag{31}$$

where $C = \sum_{d=2}^{D} \binom{N-2}{d-2} \frac{d}{\kappa_d}$

In our experiments we choose of $\kappa_d = \binom{N-2}{d-2} \frac{d(d-1)}{2}$, which conveniently returns $C = 2H_{D-1}$ (see Appendix A), with H_{D-1} being the $(D-1)$-th harmonic number. However, our theory holds true for any κ_d yielding sparse hypergraphs.

The classic effect of $\alpha(K)$ and $\beta(c)$ is summarized in Fig. 4(a), where the maximum hyperedges size is fixed to $D = 2$, hence $\gamma(D) = 1$. Here, we observe that the undetectability gap reduces when increasing c. Graphs with higher average degrees are more detectable even when there is a larger inter-community mixing. The effect of larger K is that of skewing the detectability phase transition. This is because edges contributing to c_{out} are spread over $K - 1$ communities, while those accounted for c_{in} concentrate in a single one. Intuitively, increasing K allows to have more in-out edges, and detectability is still possible because of the dominating c_{in} term. The limit value $\rho_{\mathrm{in}} = 1/K$ constitutes the perfect mixing case $c_{\mathrm{in}} = c_{\mathrm{out}} = c$, where detectability is unfeasible for any K and finite degree c. One should notice that, while the bounds drawn in Fig. 4 hold theoretically, for large K it may be exponentially hard to retrieve communities even in the detectable region [6, 48].

The higher-order effects on detectability are shown in Fig. 4(b)-(c). The presence of hyperedges with $D > 2$ enters in Eq. (31) as the product of two separate contributions, $\gamma(D) = \gamma_1(D)\gamma_2(D)$, where

$$\gamma_1(D) = \exp\left(-\mathbb{E}\left[\log \frac{2}{(|f|(|f|-1))}\right]\right) \tag{32}$$

$$\gamma_2(D) = \frac{1}{\sqrt{C(F-1)/2}}. \tag{33}$$

These two terms have contrasting effects that multiply to obtain the overall trend of $\gamma(D)$: $\gamma_1(D)$ is monotonically increasing while $\gamma_2(D)$ is monotonically decreasing. If we were to consider only the "dispersion" contribution γ_1, we would enlarge the detectability gap by increasing Φ. However, the γ_2 term factors in the increasing number of interactions observed with larger hyperedges. The result is the overall higher-order contribution to detectability $\gamma(D) = \gamma_1(D)\gamma_2(D)$, where the value of γ_2 dominates over γ_1, giving rise to the non-trivial, monotonically decreasing, profile of Fig. 4(b).

The overall effect of higher-order terms is illustrated by plotting the relative difference $\Delta\Phi(K, c, D) = (\Phi(K, c, D) - \Phi(K, c, 2))/\Phi(K, c, 2)$ for a range of c and D values, with
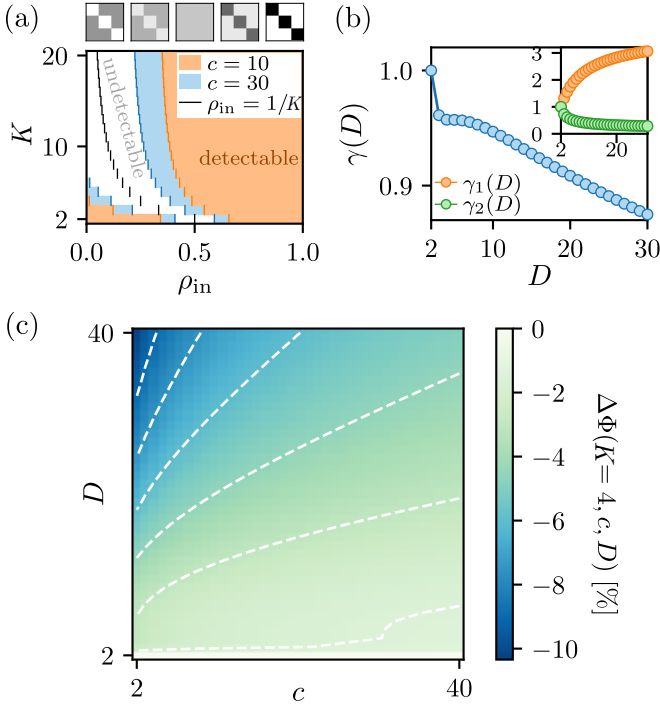
FIG. 4: **Theoretical phase transition.** Due to the decomposition of our bound in Eqs. (29)–(31) it is possible to separately describe the effects of K, c and D on the predicted phase transition. **(a)** Detectability bounds for networks ($D = 2$). Increasing c yields a broader range of detectable configurations (colored areas) for ρ_{in}. The number of communities skews detectability: while for $K = 2$ communities can be detected in extremely disassortative regimes (ρ_{in} close to zero), when more communities are present, only assortative networks are detectable. **(b)** Effect of the maximum hyperedge size D. The term $\gamma(D)$ in Eq. (31) can be split into the product $\gamma_1(D)\gamma_2(D)$, as defined in Eqs. (32)–(33). The non-trivial decrease of $\gamma(D)$ results from the interplay of $\gamma_1(D)$ and $\gamma_2(D)$, having opposite monotonicity. **(c)** The percentage decrease $\Delta\Phi(K, c, D) = (\Phi(K, c, D) - \Phi(K, c, 2))/\Phi(K, c, 2)$ in detectability for different c, D values shows that higher-order interactions steadily improve detection, especially in sparse regimes.

$K = 4$, as shown in Fig. 4(c). We observe how higher-order interactions lead to better detectability for all c, especially in sparse regimes, where c is small and pairwise information is not sufficient for the recovery of the communities.

D. Entropy and higher-order information

Hypergraphs are often compared against their clique decomposition, i.e., the graph obtained by projecting all hyperedges onto their pairwise connections, as a baseline network structure [49–51].

The clique decomposition yields highly dense graphs. For this reason, most theoretical results on sparse graphs are not directly applicable, algorithmic implementations become heavier—many times unfeasible—and storage in memory is suboptimal. Previous work also showed that algorithms developed for hypergraphs tend to work better in many practical scenarios [16]. Intuitively, hypergraphs "are more informative" than graphs [52], as there exists only one clique decomposition induced by a given hypergraph, but possibly more hypergraphs corresponding to a given clique decomposition. Here we give a theoretical basis to this common intuition and find that, within our framework, we can quantify the extra information carried by higher-order interactions.

For a given hypergraph $H = (V, E)$, edge $(i, j) \in V^2$ and hyperedge $e \in E$, we define the probability distribution

$$p_H(\{i, j\}, e) = \begin{cases} \dfrac{1}{E} \dfrac{2}{|e|(|e|-1)} & \text{if } i, j \in e \\ 0 & \text{otherwise}. \end{cases} \quad (34)$$

This distribution represents the joint probability of drawing a hyperedge uniformly at random among the possible E in the hypergraph and a dyadic interaction $\{i, j\}$ out of the possible $\binom{|e|}{2}$ within the hyperedge e. From Eq. (34) we can derive the following marginal distributions:

$$p_E(e) = \frac{1}{E} \quad (35)$$

$$p_\mathcal{C}(\{i, j\}) = \frac{1}{E} \sum_{e \in E: i, j \in e} \frac{2}{|e|(|e|-1)}, \quad (36)$$

for all $e \in E$ and pairs of nodes $i \neq j$. The distribution p_E is a uniform random draw of hyperedges. The distribution $p_\mathcal{C}$ represents the probability of drawing a weighted interaction $\{i, j\}$ in the clique decomposition of H.

With Eqs. (34)–(36) at hand, it is possible to rewrite $\gamma_1(D)$ in Eq. (32) as

$$\log \gamma_1(D) = \mathcal{H}(\{i, j\} \,|\, f), \quad (37)$$

where $\mathcal{H}(\cdot \,|\, \cdot)$ is the conditional entropy. This entropy is minimized when $p_\mathcal{C}(\{i, j\})$ is very different than $p_H(\{i, j\}|f)$, i.e., when conditioning a pair $\{i, j\}$ to be in f brings additional information with respect to the interaction $\{i, j\}$ alone. This happens when $\{i, j\}$ appears in several hyperedges and it is difficult to reconstruct the hypergraph from its clique decomposition. As lower values of γ_1 imply easier recovery, Eq. (37) suggests that recovery is favored in hypergraphs where hyperedges overlap substantially and that cannot be easily distinguished from their clique decomposition.

We obtain a similar result by rewriting Eq. (37) as

$$\gamma_1(D) = \frac{\exp \mathcal{H}(p_H)}{\exp \mathcal{H}(p_E)} = \frac{\text{PP}(p_H)}{\text{PP}(p_E)}, \quad (38)$$

which is the ratio of two exponentiated entropies. In information theory, PP is referred to as perplexity [53], and it is an effective measure of the number of possible outcomes in a probability distribution [54]. Once we fix the number of hyperedges E (and therefore $\text{PP}(p_E)$), the number of effective outcomes is given by the number of likely drawn $\{i, j\}$ pairs.

This number is minimized when there is high overlap between hyperedges, thus confirming the interpretation of Eq. (37).

Finally, we set a different focus by rewriting γ_1 as

$$\log \gamma_1(D) = \mathcal{H}(p_\mathcal{C}) - \mathrm{KL}\left(p_H \,||\, p_\mathcal{C} \otimes p_E\right) , \qquad (39)$$

where KL is the Kullback-Leibler divergence and $\otimes$ the product probability distribution. Here we pose the question: given a fixed clique decomposition and number of hyperedges, what is the hypergraph attaining the highest detectability? From the equation, such hypergraph is that with the highest $\mathrm{KL}\left(p_H \,||\, p_\mathcal{C} \otimes p_E\right) = I(\{i,j\}, f)$. In this case, the KL-divergence between a joint distribution and its marginals, also called mutual information I [55] of the two random variables, describes the information shared between pairwise interactions and single hyperedges. Hypergraphs with high KL-divergence, i.e, high information about a given $\{i,j\}$ in a single hyperedge f, will yield better detectability. In other words, it is preferable to choose hypergraphs that, while still producing the observed clique decomposition (thus achieving low entropy $\mathcal{H}(p_H)$), have largely overlapping hyperedges. The results discussed in this section provides a theoretically guidance for the construction of hypergraphs that explain an observed graph made of only pairwise interactions [56], a problem relevant in datasets where higher-oder interactions are not explicitly tracked.

V. EXPERIMENTS ON REAL DATA

Our model leads to a natural algorithmic implementation to learn communities in hypergraphs. In fact, alternating MP and EM rounds, our algorithm outputs marginal probabilities $q_i(t_i)$ for a node i to belong to a community t_i, as well as the community ratios n and the affinity matrix p. We illustrate an application of this procedure on a dataset of interactions between high school students (High School) [57]. Here, nodes are students and hyperedges represent whether a group of students was observed in close proximity, as recorded by wearable devices. The hypergraph contains $N = 327$ nodes and $E = 7818$ hyperedges. In Fig. 5(a) we show the communities inferred on the dataset where only hyperedges up to size $D = 2, 3, 4$ are kept. We observe a clear progression in how the nodes are gradually allocated into different groups when higher-order interactions are progressively taken into account. This suggests that interactions beyond pairs carry information that would get lost if only edges were to be observed.

To get a qualitative interpretation, we compare the communities inferred with the nine classes attended by the students, an attribute available with the dataset. We illustrate the hypergraph of student interactions, coloring each node according to its class, in Fig. 5(b). Previous studies have shown that in this dataset a number of interactions happen with stronger prevalence within students of the same class [57]. In Fig. 5(c), we compare the communities inferred with different maximum hyperedge size D with the classes, and observe that there is a stronger alignment between them when larger hyperedges are utilized for inference. In Fig. 5(d) we show, at $D = 2, 3, 4$, the Normalized Mutual Information (NMI) between inferred communities and class attributes, the AUC with respect to the

full dataset, and the fraction ρ_D of hyperedges with size equal to D. In addition, our algorithm detects connection patterns that were previously observed between the different student classes as captured by the affinity matrix p, see Appendix G 2 for details.

A feature that sets MP apart from other inference methods is the possibility to approximately compute the evidence $Z = p(A \,|\, p, n)$ of the whole dataset, or, equivalently, the free energy $F = -\log Z$. In Appendix G we discuss how to make the free energy computations feasible by exploiting classical cavity arguments, as well as a dynamic program similar to that employed for MP. We present the results of these estimates on the High School dataset in Fig. 5(e). Here we take the values of n and p inferred by cutting the dataset at maximum hyperedge sizes $D = 2, 3, 4$. Then, we compute the free energy on the full dataset ($D = 5$) in the simplex of n, p parameters outlined by the three vertices. We notice that interactions of size $D = 5$ seem to be less informative and lead to suboptimal inference, see Appendix G 3. Similarly to what observed on graphs [6], the energy landscape appears rugged and complex. EM converges to solutions that are local attraction points, i.e., valleys of low-energy configurations. Moreover, the free energy of the p, n parameters inferred with only pairwise interactions (i.e., $D = 2$, lower-right) is higher than that inferred for $D = 3$ (upper-left), which is in turn higher that the one of $D = 4$ (bottom-left).

VI. CONCLUSION

We developed a probabilistic generative model and a message-passing-based inference procedure that lead to several results advancing community detection on hypergraphs. In particular we obtained closed-form bounds for the detectability of community configurations, extending the seminal results of Decelle *et al.* [6] to higher-order interactions. Experimental validation of such bounds shows the emergence of a detectability phase transition when spanning from disassortative to assortative community structures. With these theoretical bounds at hand, we investigate the relationship between hypergraphs and graphs from an information-theoretical perspective. Characterizing the entropy and perplexity of pairs of nodes in hyperedges, we find that hypergraphs with many overlapping hyperedges are easier to detect. Beside these theoretical advancements, we develop two relevant algorithmic ones. First, we derive an efficient and scalable Message-Massing algorithm to learn communities and model parameters. Second, we propose an exact and efficient sampling routine that generates synthetic data with desired community structure according to our probabilistic model in order of seconds. Both of these implementations are released open source [42].

The mathematical tools we propose here to obtain our results are valid for standard hypergraphs. We can foresee that they could be generalized to dynamic hypergraphs where interactions change in time, using intuitions derived for dynamic graphs [10]. Similarly, it would be interesting to see how detectability bounds change when accounting for node attributes, as results in networks have shown that adding extra informa-
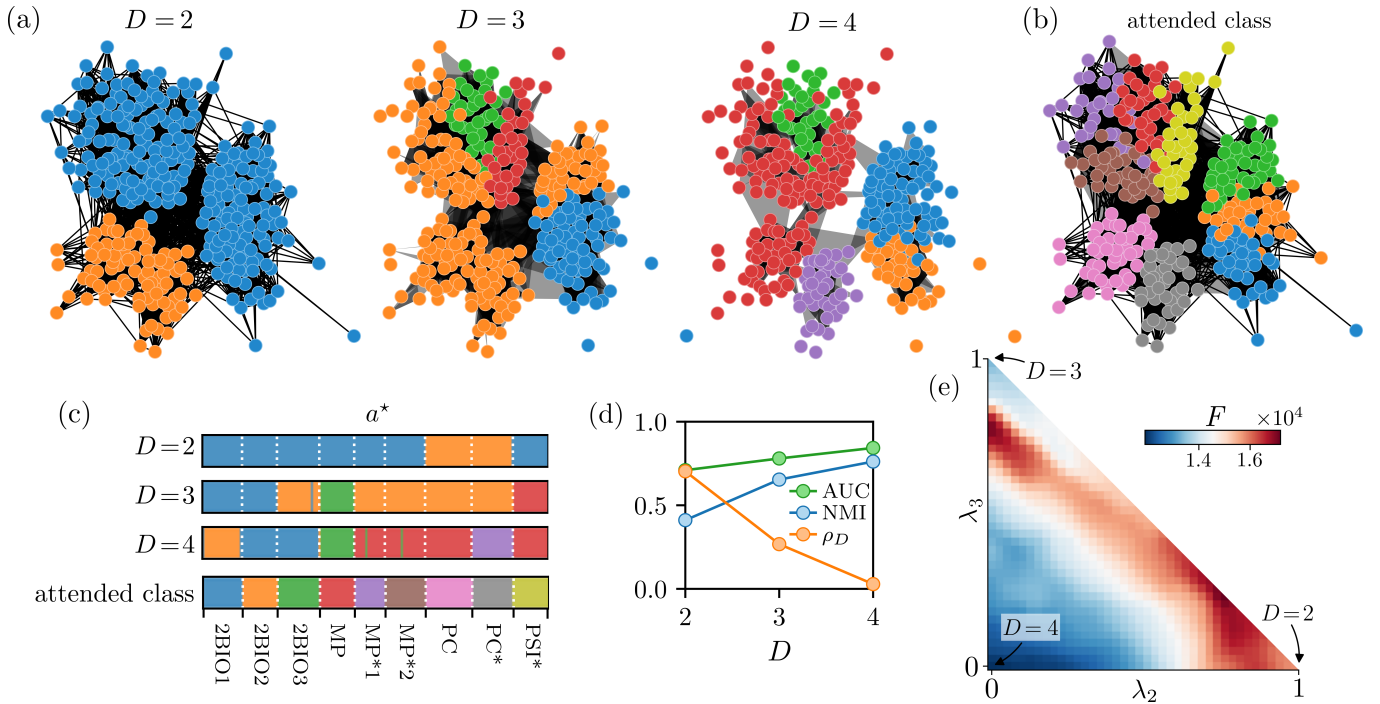
FIG. 5: . We infer the communities via MP and EM on the High School dataset. In all cases, we run inference with $K = 10$ communities. **(a)** Inferred communities on the High School dataset, only utilizing hyperedges up to a maximum size D. Taking into account higher-order information, up to $D = 4$, results in more granular partitions. **(b)** Graphical representation of the students' partition into classes. We draw only hyperedges of size D. **(c)** We compare the inferred partitions with the "attended class" covariate of the nodes, i.e., the classes students participate in. We comment further on this comparison in Appendix G 2. **(d)** A quantitative measurement complementing that of panel (b): the Normalized Mutual Information (NMI) between inferred communities and attended classes, the AUC on the full dataset, as well as the ratio ρ_D of hyperedges of size equal to D. **(e)** Free energy landscape. We consider the parameters (p_2, n_2), (p_3, n_3) and (p_4, n_4) inferred from the dataset with, respectively, $D = 2, 3, 4$. With these, we build the simplex of convex combinations $p = \sum_{i \in \{2,3,4\}} \lambda_i p_i$, where $\sum_{i \in \{2,3,4\}} \lambda_i = 1$ and $0 \leq \lambda_i \leq 1$ (similarly for n). For every point in the simplex, we compute the free energy on the full dataset, i.e., with $D = 5$. More details on these computations are provided in Appendix G 1.

tion can boost community detection [58–60]. Finally, from an empirical perspective, it would be interesting to see how our theoretical insights in terms of entropy of hypergraphs and clique expansion match measures that relate hypergraphs to simplicial complexes [61].

ACKNOWLEDGMENTS

Appendix A: Expected degree and choice of κ_d

As we commented in Sec. II, the choice of the normalizing constant κ_d, for $d = 2, \ldots, D$, controls the Bernoulli probabilities for all hyperedges $e \in \Omega$ via

$$\mathbb{P}(e \,|\, p, t) = \frac{\pi_e}{\kappa_{|e|}} = \frac{\sum_{i<j \in e} p_{t_i t_j}}{\kappa_{|e|}}.$$

Our theoretical analysis and results hold for general choices of κ_d, as long as these respect the following conditions. First, for any choice of a symmetric $0 \leq p_{ab} \leq 1$, we need valid probabilities $0 \leq \pi_e/\kappa_{|e|} \leq 1$. This implies that, necessarily:

$$\kappa_d \geq \frac{d(d-1)}{2} \quad \forall d = 2, \ldots, D. \tag{A1}$$

Second, we want the ensemble to consist of sparse hypergraphs, in expectation. A good proxy for such a requirement is the average degree, which we can compute explicitly:

$$
\begin{aligned}
\langle d \rangle &= \frac{1}{N} \sum_{i \in V} \sum_{e \in \Omega : i \in e} \mathbb{P}(e \,|\, p, t) \\
&= \frac{1}{N} \sum_{e \in \Omega} \sum_{i \in e} \mathbb{P}(e \,|\, p, t) \\
&= \frac{1}{N} \sum_{e \in \Omega} |e| \mathbb{P}(e \,|\, p, t) \\
&= \frac{1}{N} \sum_{e \in \Omega} \frac{|e|}{\kappa_{|e|}} \sum_{i < j \in e} p_{t_i t_j} \\
&= \frac{C}{N} \sum_{i < j \in V} p_{t_i t_j} \\
&\approx \frac{C}{N} \sum_{a \leq b \in [K]} \frac{p_{ab}(N n_a)(N n_b)}{1 + \delta_{ab}} \\
&= \frac{C}{2} \sum_{a, b \in [K]} c_{ab} n_a n_b \,,
\end{aligned}
\tag{A2}
$$

where

$$
C = \sum_{d=2}^{D} \binom{N - 2}{d - 2} \frac{d}{\kappa_d} \,.
$$

We assume $c_{ab} = O(1)$, i.e. to be in a sparse regime. Thus, the expected degree's scale is governed by C and, in turn, by the choice of κ_d, as

$$
\langle d \rangle = O(C) \,.
$$

Additionally, but not necessarily, we wish our model to extend the classical SBM, which imposes the additional condition $\kappa_2 = 1$. There exist many choices of κ_d obeying the constraints just discussed. A natural one is the minimum value satisfying Eq. (A1), i.e. $\kappa_d = d(d - 1)/2$. This gives

$$
C = \frac{2}{N - 1} \sum_{d=1}^{D-1} \binom{N - 1}{d}
$$

that, for $D = N$, returns $\langle d \rangle = O\left(2^N / (N - 1)\right)$, which is too high to yield sparse hypergraphs. Notice that, in practice, we rarely use $D = N$. However, such considerations are useful to evaluate how different κ_d values reflect on the properties of the hypergraphs ensembles of the model.

A more interesting choice is given by

$$
\kappa_d = \frac{d(d - 1)}{2} \binom{N - 2}{d - 2} \,.
$$

This corresponds to taking the average among the $d(d - 1)/2$ interactions that yield π_e, and $\binom{N-2}{d-2}$ is a normalization: once observed an interaction between two nodes i, j, the remaining $d - 2$ are chosen at random. This gives

$$
\begin{aligned}
C &= 2 \sum_{d=1}^{D-1} \frac{1}{d} \\
&= 2 H_{D-1} \,,
\end{aligned}
\tag{A3}
$$

which is proportional to the $(D - 1)$-th harmonic number, hence growing more mildly at leading order as $C = O(\log D)$. Aside from having an interpretation in terms of null modeling, the value in Eq. (A3), which we utilize experimentally, was shown to be a sensible choice in many real-life scenarios [17, 41].

Appendix B: Message-Passing derivations

MP equations have been developed in the case of general factor graphs, see for example Murphy et al. [35], Section 22.2.3.2. We consider approximate messages from hyperedges e to nodes i being $\widehat{q}_{e \to i}(t_i)$, and vice versa, $q_{i \to e}(t_i)$. The messages, for any $e \in \mathcal{F}, i \in \partial e$ satisfy the general updates

$$
\begin{aligned}
q_{i \to e}(t_i) &\propto n_{t_i} \prod_{f \in \partial i \setminus e} \widehat{q}_{f \to i}(t_i) \\
\widehat{q}_{e \to i}(t_i) &\propto \sum_{t_j : j \in \partial e \setminus i} \left(\frac{\pi_e}{\kappa_e} \right)^{A_e} \left(1 - \frac{\pi_e}{\kappa_e} \right)^{1 - A_e} \prod_{j \in \partial e \setminus i} q_{j \to e}(t_j) \, .
\end{aligned} \tag{B1}
$$

The marginal beliefs are given by

$$
q_i(t_i) \propto n_{t_i} \prod_{e \in \partial i} \widehat{q}_{e \to i}(t_i) \, . \tag{B2}
$$

1. Message updates

First, we can distinguish the values of messages for function nodes e such that $A_e = 0$ or $A_e = 1$, i.e. if the hyperedge e is observed or not in the data.

If $A_e = 1$, i.e. $e \in E$, then

$$
\begin{aligned}
\widehat{q}_{e \to i}(t_i) &\propto \sum_{t_j : j \in \partial e \setminus i} \frac{\pi_e}{\kappa_e} \prod_{j \in \partial e \setminus i} q_{j \to e}(t_j) \\
&\propto \sum_{t_j : j \in \partial e \setminus i} \pi_e \prod_{j \in \partial e \setminus i} q_{j \to e}(t_j) \, .
\end{aligned} \tag{B3}
$$

If $A_e = 0$, then $e \in \Omega \setminus E$. We start by computing

$$
\begin{aligned}
\widehat{q}_{e \to i}(t_i) &\propto \sum_{t_j : j \in \partial e \setminus i} \left(1 - \frac{\pi_e}{\kappa_e} \right) \prod_{j \in \partial e \setminus i} q_{j \to e}(t_j) \\
&= \sum_{t_j : j \in \partial e \setminus i} \prod_{j \in \partial e \setminus i} q_{j \to e}(t_j) - \sum_{t_j : j \in \partial e \setminus i} \frac{\pi_e}{\kappa_e} \prod_{j \in \partial e \setminus i} q_{j \to e}(t_j) \\
&= 1 - \sum_{t_j : j \in \partial e \setminus i} \frac{\pi_e}{\kappa_e} \prod_{j \in \partial e \setminus i} q_{j \to e}(t_j) \\
&= 1 - \frac{1}{N} \sum_{t_j : j \in \partial e \setminus i} \frac{\sum_{k < m \in e} c_{t_k t_m}}{\kappa_e} \prod_{j \in \partial e \setminus i} q_{j \to e}(t_j) \, .
\end{aligned} \tag{B4}
$$

We indicate with $\hat{Z}_{e \to i}(t_i)$ the convenient non-normalized rewriting of $\widehat{q}_{e \to i}(t_i)$ in Eq. (B4). Therefore, we find

$$
\begin{aligned}
q_{i \to e}(t_i) &\propto n_{t_i} \prod_{f \in \partial i \setminus e} \widehat{q}_{f \to i}(t_i) \\
&= \frac{n_{t_i}}{\widehat{q}_{e \to i}(t_i)} \prod_{f \in \partial i} \widehat{q}_{f \to i}(t_i) \tag{B5} \\
&\propto \frac{n_{t_i}}{\hat{Z}_{e \to i}(t_i)} \prod_{f \in \partial i} \widehat{q}_{f \to i}(t_i) \tag{B6} \\
&= \frac{q_i(t_i)}{\hat{Z}_{e \to i}(t_i)} \, , \tag{B7}
\end{aligned}
$$

where from the Eq. (B5) to Eq. (B6) we used $\hat{Z}_{e\to i}(t_i)$ introduced in Eq. (B4). We evaluate the expression in Eq. (B7) for the limit $N \to +\infty$, which gives the node-to-hyperedge messages for $e \in \Omega \setminus E$ as

$$q_{i\to e}(t_i) = q_i(t_i) + O\left(\frac{1}{N}\right)$$

$$\approx q_i(t_i), \tag{B8}$$

i.e., the nodes approximately (to leading order in $O(1/N)$) share their marginal belief to hyperedges that are not observed in the data. Using Eq. (B8), we can also approximate Eq. (B4) as

$$\hat{q}_{e\to i}(t_i) \propto 1 - \frac{1}{N} \sum_{t_j : j \in \partial e \setminus i} \frac{\sum_{k < m \in e} c_{t_k t_m}}{\kappa_e} \prod_{j \in \partial e \setminus i} q_{j\to e}(t_j)$$

$$\approx 1 - \frac{1}{N} \sum_{t_j : j \in \partial e \setminus i} \frac{\sum_{k < m \in e} c_{t_k t_m}}{\kappa_e} \prod_{j \in \partial e \setminus i} q_j(t_j). \tag{B9}$$

In the assumed sparsity regime, the term of order $O(1/N)$ in Eq. (B9) is close to zero. Since for $x \approx 0$ the approximation $1 - x \approx e^{-x}$ is sufficiently accurate, we write

$$\hat{q}_{e\to i}(t_i) \approx \exp\left(-\frac{1}{N} \sum_{t_j : j \in \partial e \setminus i} \frac{\sum_{k < m \in e} c_{t_k t_m}}{\kappa_e} \prod_{j \in \partial e \setminus i} q_j(t_j)\right). \tag{B10}$$

We can put the hyperedge-to-node updates together using the two results in Eq. (B3) and in Eq. (B10). Specifically, we derive the following expression for the message $q_{i\to e}(t_i)$, where $e \in E$:

$$q_{i\to e}(t_i) \propto n_{t_i} \prod_{\substack{f \in \Omega : \\ f \in \partial i \setminus e}} \hat{q}_{f\to i}(t_i)$$

$$= n_{t_i} \prod_{\substack{f \in E : \\ f \in \partial i \setminus e}} \hat{q}_{f\to i}(t_i) \prod_{\substack{f \in \Omega \setminus E \\ f \in \partial i}} \hat{q}_{f\to i}(t_i)$$

$$\approx n_{t_i} \left(\prod_{\substack{f \in E : \\ f \in \partial i \setminus e}} \hat{q}_{f\to i}(t_i)\right) \left[\prod_{\substack{f \in \Omega \setminus E : \\ f \in \partial i}} \exp\left(-\frac{1}{N} \sum_{t_j : j \in \partial f \setminus i} \frac{\sum_{k < m \in f} c_{t_k t_m}}{\kappa_f} \prod_{j \in \partial f \setminus i} q_j(t_j)\right)\right] \tag{B11}$$

$$= n_{t_i} \left(\prod_{\substack{f \in E : \\ f \in \partial i \setminus e}} \hat{q}_{f\to i}(t_i)\right) \exp\left(-\frac{1}{N} \sum_{\substack{f \in \Omega \setminus E : \\ f \in \partial i}} \sum_{t_j : j \in \partial f \setminus i} \frac{\sum_{k < m \in f} c_{t_k t_m}}{\kappa_f} \prod_{j \in \partial f \setminus i} q_j(t_j)\right)$$

$$\approx n_{t_i} \left(\prod_{\substack{f \in E : \\ f \in \partial i \setminus e}} \hat{q}_{f\to i}(t_i)\right) \exp\left(-\frac{1}{N} \sum_{\substack{f \in \Omega : \\ f \in \partial i}} \sum_{t_j : j \in \partial f \setminus i} \frac{\sum_{k < m \in f} c_{t_k t_m}}{\kappa_f} \prod_{j \in \partial f \setminus i} q_j(t_j)\right) \tag{B12}$$

$$= n_{t_i} \left(\prod_{\substack{f \in E : \\ f \in \partial i \setminus e}} \hat{q}_{f\to i}(t_i)\right) \exp(-h_i(t_i)). \tag{B13}$$

In Eq. (B11), we used the approximation introduced in Eq. (B10). In Eq. (B12) we passed from summing over $\Omega \setminus E$ to Ω. This approximation is sensible as long as the expected degree of the nodes grows at most as N, which is satisfied in the assumed sparse regime, as discussed in Appendix A. Finally, in Eq. (B13) we introduced node-dependent external field $h_i(t_i)$ whose definition naturally follows from the argument of the exponential in Eq. (B12).

2. External field updates

We simplify the external field to remove the node dependency of $h_i(a)$. The node-dependent external field reads

$$
h_i(t_i) = \frac{1}{N} \sum_{f \in \partial i} \frac{1}{\kappa_f} \left(\sum_{t_j : j \in \partial f \backslash i} \sum_{k < m \in f} c_{t_k t_m} \prod_{r \in f \backslash i} q_r(t_r) \right)
$$

$$
= \frac{1}{N} \sum_{f \in \partial i} \frac{1}{\kappa_f} \left(\sum_{t_j : j \in f \backslash i} \sum_{m \in f \backslash i} c_{t_i t_m} \prod_{r \in f \backslash i} q_r(t_r) \right) + \text{const.}
\tag{B14}
$$

The sum in parentheses in Eq. (B14) can be simplified as

$$
\sum_{t_j : j \in f \backslash i} \left[\left(\sum_{m \in f \backslash i} c_{t_i t_m} \right) \prod_{r \in f \backslash i} q_r(t_r) \right] = \sum_{t_j : j \in f \backslash i} \sum_{m \in f \backslash i} \left(c_{t_i t_m} \prod_{r \in f \backslash i} q_r(t_r) \right)
$$

$$
= \sum_{m \in f \backslash i} \sum_{t_j : j \in f \backslash i} \left(c_{t_i t_m} \prod_{r \in f \backslash i} q_r(t_r) \right)
$$

$$
= \sum_{m \in f \backslash i} \sum_{t_m} c_{t_i t_m} q_m(t_m) \,.
\tag{B15}
$$

Plugging Eq. (B15) into Eq. (B14) we get, ignoring constants,

$$
h_i(t_i) = \frac{1}{N} \sum_{f \in \partial i} \frac{1}{\kappa_f} \sum_{m \in f \backslash i} \sum_{t_m} c_{t_i t_m} q_m(t_m)
$$

$$
= \frac{C'}{N} \sum_{j \in V \backslash i} \sum_{t_j} c_{t_i t_j} q_j(t_j)
$$

$$
\approx \frac{C'}{N} \sum_{j \in V} \sum_{t_j} c_{t_i t_j} q_j(t_j) \,,
\tag{B16}
$$

with $C' = \sum_{d=2}^{D} \binom{N-2}{d-2} \frac{1}{\kappa_d}$ and where in Eq. (B16) we included i in the node summation. Since Eq. (B16) does not depend on i, we define the node-independent external field

$$
h(a) = \frac{C'}{N} \sum_{j \in V} \sum_{t_j} c_{a t_j} q_j(t_j) \quad \forall a \in [K] \,.
$$

3. Marginal beliefs updates

Notice, that, in passing from Eq. (B11) to Eq. (B13) and then in Eq. (B17), we have shown that

$$
\prod_{\substack{f \in \Omega \backslash E \\ f \in \partial i}} \widehat{q}_{f \to i}(t_i) \approx \exp(-h_i(t_i)) \approx \exp(-h(t_i)) \,.
\tag{B17}
$$

We use the same argument to treat the general expression of the marginal beliefs in Eq. (B2), yielding

$$
q_i(t_i) \propto n_{t_i} \prod_{e \in \partial i} \widehat{q}_{e \to i}(t_i)
$$

$$
= n_{t_i} \prod_{\substack{e \in E: \\ e \in \partial i}} \widehat{q}_{e \to i}(t_i) \prod_{\substack{e \in \Omega \backslash E: \\ e \in \partial i}} \widehat{q}_{e \to i}(t_i)
$$

$$
\approx n_{t_i} \prod_{\substack{e \in E: \\ e \in \partial i}} \widehat{q}_{e \to i}(t_i) \exp(-h(t_i)) \,.
$$

4. Summary: approximate Message-Passing updates

Putting all derivations together, the final MP equations read

$$\text{Node-to-observed hyperedge:} \quad q_{i \to e}(t_i) \propto n_{t_i} \left(\prod_{\substack{f \in E \\ f \in \partial i \setminus e}} \widehat{q}_{f \to i}(t_i) \right) \exp(-h(t_i)) \quad \forall e \in E, i \in e$$

$$\text{Observed hyperedge-to-node:} \quad \widehat{q}_{e \to i}(t_i) \propto \sum_{t_j : j \in \partial e \setminus i} \pi_e \prod_{j \in \partial e \setminus i} q_{j \to e}(t_j) \quad \forall e \in E, i \in e \tag{B18}$$

$$\text{External field:} \quad h(t_i) = \frac{C'}{N} \sum_{j \in V} \sum_{t_j} c_{t_i t_j} q_j(t_j) \tag{B19}$$

$$\text{Marginals:} \quad q_i(t_i) \propto n_{t_i} \left(\prod_{\substack{f \in E \\ f \in \partial i}} \widehat{q}_{f \to i}(t_i) \right) \exp(-h(t_i)).$$

Notice that the MP updates cannot be naively implemented as presented. In fact, the update in Eq. (B18) for $\widehat{q}_{e \to i}(t_i)$ have cost $O(K^{|e|-1})$, which does not scale with the hyperedge size. In Appendix D we present a dynamic programming approach to perform this computation exactly with cost $O(K^2 |e|)$, and comment on further algorithmic details to implement the MP updates in practice.

Appendix C: Expectation-Maximization inference

Updates of the community priors n. We take the derivative of the log-likelihood in Eq. (4). By imposing the constraint $\sum_{a=1}^{K} n_a = 1$, we obtain the update in Eq. (13).
Updates of the affinity matrix p. We show here the updates in terms of c. These easily translate to those in terms of the affinity matrix p as the expression we derive below in Eq. (C6) is invariant with respect to the substitution $c = Np$. Let $x_e = \sum_{i<j \in e} c_{t_i t_j} / N\kappa_e$. Then, ignoring additive constants, the log-likelihood reads

$$
\begin{aligned}
\mathcal{L} &= \sum_{e \in E} \log \left(\sum_{i<j \in e} c_{t_i t_j} \right) + \sum_{e \in \Omega \setminus E} \log(1 - x_e) \\
&\approx \sum_{e \in E} \log \left(\sum_{i<j \in e} c_{t_i t_j} \right) - \sum_{e \in \Omega \setminus E} x_e \\
&= \sum_{e \in E} \log \left(\sum_{i<j \in e} c_{t_i t_j} \right) - \sum_{e \in \Omega \setminus E} \frac{\sum_{i<j \in e} c_{t_i t_j}}{N \kappa_e}
\end{aligned}
\tag{C1}
$$

where Eq. (C1) is the linearization of $\log(1-x) \approx x$ around $x = 0$, which is valid at leading order $O(1/N)$. We now take a variational approach to find a lower bound $\tilde{\mathcal{L}}$ of the log-likelihood:

$$
\begin{aligned}
\mathcal{L} &\approx \sum_{e \in E} \log \left(\sum_{i<j \in e} c_{t_i t_j} \right) - \sum_{e \in \Omega \setminus E} \frac{\sum_{i<j \in e} c_{t_i t_j}}{N \kappa_e} \\
&\geq \sum_{e \in E} \sum_{i<j \in e} \rho_{ij}^e \log \left(\frac{c_{t_i t_j}}{\rho_{ij}^e} \right) - \sum_{e \in \Omega \setminus E} \frac{\sum_{i<j \in e} c_{t_i t_j}}{N \kappa_e} \\
&= \sum_{e \in E} \sum_{i<j \in e} \rho_{ij}^e \log c_{t_i t_j} - \sum_{e \in \Omega \setminus E} \frac{\sum_{i<j \in e} c_{t_i t_j}}{N \kappa_e} + \text{const.} \\
&= \tilde{\mathcal{L}}(c) + \text{const.},
\end{aligned}
\tag{C2}
$$

which is valid for any distribution ρ_{ij}^e such that $\sum_{i<j\in e} \rho_{ij}^e = 1$. In Eq. (C2), we utilized Jensen's inequality. The lower bound is exact when

$$\rho_{ij}^e = \frac{c_{t_i t_j}}{\sum_{i<j\in e} c_{t_i t_j}} = \frac{c_{t_i t_j}}{N\pi_e} \quad . \tag{C3}$$

We compute the derivative of the variational lower bound and approximate to leading terms in N:

$$\begin{aligned}
\frac{\partial \tilde{\mathcal{L}}}{\partial c_{ab}} &= \frac{1}{c_{ab}} \sum_{e\in E} \sum_{i<j\in e} \rho_{ij}^e \delta_{t_i a}\delta_{t_j b} - \frac{1}{N}\sum_{e\in\Omega\setminus E} \frac{1}{\kappa_e} \sum_{i<j\in e} \delta_{t_i a}\delta_{t_j b} \\
&\approx \frac{1}{c_{ab}} \sum_{e\in E} \sum_{i<j\in e} \rho_{ij}^e \delta_{t_i a}\delta_{t_j b} - \frac{1}{N}\sum_{e\in\Omega} \frac{1}{\kappa_e} \sum_{i<j\in e} \delta_{t_i a}\delta_{t_j b} \tag{C4} \\
&= \frac{1}{c_{ab}} \sum_{e\in E} \sum_{i<j\in e} \rho_{ij}^e \delta_{t_i a}\delta_{t_j b} - \frac{C'}{N}\sum_{i<j\in V} \delta_{t_i a}\delta_{t_j b} \\
&= \frac{1}{c_{ab}} \sum_{e\in E} \sum_{i<j\in e} \rho_{ij}^e \delta_{t_i a}\delta_{t_j b} - \frac{C'}{2N}(N_a N_b - \delta_{ab}N_a) \\
&= \frac{1}{c_{ab}} \sum_{e\in E} \sum_{i<j\in e} \rho_{ij}^e \delta_{t_i a}\delta_{t_j b} - \frac{C'}{2}(Nn_a n_b - \delta_{ab}n_a) . \tag{C5}
\end{aligned}$$

where $C' = \sum_{d=2}^{D} \binom{N-2}{d-2}\frac{1}{\kappa_d}$. Notice that the approximations in Eq. (C4) and Eq. (C5) hold valid only when considering c_{ab} in the expressions, as by assumption $c = O(1)$. Now, by setting Eq. (C5) equal to zero, and substituting ρ_{ij}^e from Eq. (C3), we obtain the update

$$c_{ab}^{(t+1)} = c_{ab}^{(t)} \frac{2\sum_{e\in E} \#_{ab}^e/\pi_e}{N\,C'\,(Nn_a n_b - \delta_{ab}n_a)} , \tag{C6}$$

where $\#_{ab}^e = \sum_{i<j\in e} \delta_{t_i a}\delta_{t_j b}$.

Appendix D: Algorithmic and computational details

1. Dynamic programming for MP

In this section, we explain how the MP updates for the $\widehat{q}_{e\to i}(t_i)$ messages can be performed efficiently. In log-space, the messages can be compactly written as

$$\begin{aligned}
\log \widehat{q}_{e\to i}(t_i) &= \log \sum_{t_j:j\in\partial e\setminus i} \pi_e \prod_{j\in e\setminus i} q_{j\to e}(t_j) + \text{const.} \\
&= \psi(e, i, t_i) + \text{const.} \quad . \tag{D1}
\end{aligned}$$

Below, we focus on finding efficient updates for ψ as defined in Eq. (D1), which should be exponentiated and properly normalized to find the original messages $\widehat{q}_{e\to i}(t_i)$. For this, we introduce an auxiliary quantity. For any subset $g \subseteq f$ of nodes in f, where $i \in g$, we define

$$\eta(g, i, t_i) = \log\left[\sum_{t_j:j\in g\setminus i} \left(\sum_{l<m\in g} p_{t_l t_m}\right) \prod_{j\in g\setminus i} q_{j\to f}(t_j)\right] .$$

Hence $\eta(f, i, t_i) = \psi(f, i, t_i) + \text{const.}$. This quantity is useful in that it allows to obtain an efficient recursion formula for ψ, by computing the η values starting from subsets g containing two nodes.

Without loss of generality, consider $f = \{1, \dots, m-1\}$ and $i = 1$. Consider $g = \{1, \dots, n-1\}$ for some $n \leq m$. We want

to compute η for the set $\{1, \ldots n\}$. Its exponential is given by:

$$\exp\left(\eta(\{1,\ldots,n\},1,t_1)\right) = \sum_{t_n}\sum_{t_2}\sum_{t_3}\cdots\sum_{t_{n-1}}\left(p_{t_1 t_2} + \ldots + p_{t_{n-2}t_{n-1}} + p_{t_1 t_n} + p_{t_2 t_n} + \ldots + p_{t_{n-1}t_n}\right)$$

$$\times\left(q_{2\to f}(t_2)\ldots q_{n-1\to f}(t_{n-1})q_{n\to f}(t_n)\right)$$

$$= \sum_{t_n} q_{n\to f}(t_n)\left(\sum_{t_2}\sum_{t_3}\cdots\sum_{t_{n-1}}(p_{t_1 t_2} + \ldots + p_{t_{n-2}t_{n-1}})(q_{2\to f}(t_2)\ldots q_{n-1\to f}(t_{n-1}))\right.$$

$$+ \sum_{t_2}\sum_{t_3}\cdots\sum_{t_{n-1}} p_{t_1 t_n}(q_{2\to f}(t_2)\ldots q_{n-1\to f}(t_{n-1}))$$

$$\left. + \sum_{t_2}\sum_{t_3}\cdots\sum_{t_{n-1}}(p_{t_2 t_n} + \ldots + p_{t_{n-1}t_n})(q_{2\to f}(t_2)\ldots q_{n-1\to f}(t_{n-1}))\right)$$

$$= \sum_{t_n} q_{n\to f}(t_n)\left(\exp(\eta(\{1,\ldots,n-1\},1,t_1))\right.$$

$$+ p_{t_1 t_n}$$

$$\left. + \sum_{t_2} p_{t_2 t_n} q_{2\to f}(t_2) + \ldots + \sum_{t_{n-1}} p_{t_{n-1}t_n} q_{n-1\to f}(t_{n-1})\right)$$

$$= \exp(\eta(\{1,\ldots,n-1\},1,t_1))$$

$$+ \sum_{t_n} q_{n\to f}(t_n)\left(p_{t_1 t_n} + \sum_{t_2} p_{t_2 t_n} q_{2\to f}(t_2) + \ldots + \sum_{t_{n-1}} p_{t_{n-1}t_n} q_{n-1\to f}(t_{n-1})\right). \tag{D2}$$

The recursion in Eq. (D2) allows to compute the value of $\eta(\{1,\ldots,n\},1,t_1)$ from $\eta(\{1,\ldots,n-1\},1,t_1)$ in time $O((n-2)K^2)$. However, we can further reduce the cost. For any $a \in [K]$, define

$$s_n(a) = \sum_{t_2} p_{t_2 a} q_{2\to f}(t_2) + \ldots + \sum_{t_{n-1}} p_{t_{n-1}a} q_{n-1\to f}(t_{n-1}).$$

Substituting the definition of $s_n(a)$ in Eq. (D2), we obtain the final two-step dynamic update:

$$s_n(a) = s_{n-1}(a) + \sum_{t_{n-1}} p_{t_{n-1}a} q_{n-1\to f}(t_{n-1}) \tag{D3}$$

$$\exp\left(\eta(\{1,\ldots,n\},1,t_1)\right) = \exp(\eta(\{1,\ldots,n-1\},1,t_1))$$

$$+ \sum_{t_n} q_{n\to f}(t_n)\left(p_{t_1 t_n} + s_n(t_n)\right). \tag{D4}$$

This yields a cost of $O(K)$ per recursion, and a total cost of $O(K|f|)$ to compute the final $\psi(f,1,t_1)$. In practice, for any e,i pair, we compute $\psi(e,i,t_i)$ for all values $t_i \in [K]$, which yields a total cost of $O(K^2|f|)$.

2. Implementation details

In our implementation of the MP and EM routines, we take some additional steps to ensure convergence to non-trivial local optima of the free energy landscape.

The initialization of the messages is performed taking into account the circular relationships in Eqs. (9)–(12). We perform them as follows: (i) randomly initialize the messages $q_{i\to e}(t_i)$. For every i,e pair, the messages are drawn from a K-dimensional Dirichlet distribution. (ii) Similarly, randomly initialize the marginal beliefs $q_i(t_i)$. (iii) We infer all the other quantities from the initialized $q_{i\to e}(t_i)$ and $q_i(t_i)$. In fact, up to constants

$$\hat{q}_{e\to i}(t_i) = \frac{q_i(t_i)}{q_{i\to e}(t_i)}.$$

All values are then normalized to have unitary sum. (iv) Finally, the external field is entirely determined by the marginals, as per Eq. (12).

We check for convergence of the MP and EM inference routines by evaluating the absolute difference between parameters in consecutive steps. We present complete pseudocodes of the two routines in Algorithm 1 and Algorithm 2.

Algorithm 1 Inferring communities (MP)

Inputs: convergence threshold ϵ_{mp}
         maximum iterations $\mathrm{iter}_{\mathrm{mp}}$
         prior n, rescaled affinity c

Randomly initialize all $q_{i \to e}(t_i), \widehat{q}_{e \to i}(t_i), q_i(t_i), h(t_i)$

for step $= 1, \ldots, \mathrm{iter}_{\mathrm{mp}}$ **do**
    // Perform updates
    for all $e \in E, i \in e, t_i \in [K]$ **do**
        update messages $q_{i \to e}(t_i)$ ▷ Eq. (9)
    end for
    for all $e \in E, i \in e, t_i \in [K]$ **do**
        update messages $\widehat{q}_{e \to i}(t_i)$ ▷ Eq. (10)
    end for
    for all $e \in E, i \in e, t_i \in [K]$ **do**
        $q_i^{old}(t_i) \leftarrow q_i(t_i)$
        update marginals $q_i(t_i)$ ▷ Eq. (11)
    end for
    for $t_i \in [K]$ **do**
        update external field $h(t_i)$ ▷ Eq. (12)
    end for

    // Check for convergence
    $\Delta = \sum_{i=1}^{N} \sum_{t_i=1}^{K} |q_i^{\mathrm{old}}(t_i) - q_i(t_i)|$
    if $\Delta < \epsilon_{\mathrm{mp}}$ **then**
        break
    end if
end for

Algorithm 2 Inferring model parameters (EM)

Inputs: convergence threshold ϵ_{em}
         maximum iterations $\mathrm{iter}_{\mathrm{em}}$

Randomly initialize c, n

for step $= 1, \ldots, \mathrm{iter}_{\mathrm{em}}$ **do**
    // Perform updates
    Perform Message-Passing inference   ▷ Algorithm 1
    $n^{\mathrm{old}} \leftarrow n$
    update n ▷ Eq. (13)
    $c^{\mathrm{old}} \leftarrow c$
    update c ▷ Eq. (14)

    // Check for convergence
    $\Delta = \sum_{a=1}^{K} |n_a - n_a^{\mathrm{old}}| + \sum_{a,b=1}^{K} |c_{ab} - c_{ab}^{\mathrm{old}}|$
    if $\Delta < \epsilon_{\mathrm{em}}$ **then**
        break
    end if
end for

While Algorithm 1 is presented as a completely parallel implementation of the MP equations Eqs. (9)–(12), in practice we proceed in batches. In fact, we find that applying completely parallel updates, i.e. applying Eq. (9) for all i, e pairs, successively Eq. (10) for all i, e pairs, and then Eq. (11) for all nodes $i \in V$, results in fast convergence to degenerate fixed-points where all nodes are assigned to the same community. For this reason, we apply dropout. Given a fraction $\alpha \in (0, 1]$, we select a random fraction α of all possible i, e pairs, and apply the update in Eq. (9) only for the selected pairs. We perform a new random draw, and update according to Eq. (10), and similarly for Eq. (11). Finally, we update the external field in Eq. (12). Empirically, we find that a value of $\alpha = 0.25$ works for synthetic data, where inference is simpler. Values below work as well. For real data we find that substantially lowering α yields more stable inference. On real data, where we alternate MP and EM, and learning is less stable, we utilize $\alpha = 0.01$. In practice, we also set a patience parameter, and only stop MP once a given number of iterations in a row falls below the threshold ϵ_{mp} in Algorithm 1. For real datasets, we set the patience to 50 consecutive steps, and the maximum number of iterations $\mathrm{iter}_{mp} = 2000$.

Appendix E: Sampling from the generative model

1. The algorithm

In the following, we describe an exact sampling procedure derived from our probabilistic model. The key observation to obtain an efficient algorithm is that the hyperedge probabilities do not depend on the nodes they contain, but only on their community assignments, as implied by Eq. (3).

For a hyperedge e and community $a \in [K]$, we define the quantity

$$\#_a^e = \sum_{i \in e} \delta_{t_i a} \, ,$$

which is the count of nodes in e that belong to community a. Crucially, the hyperedge probability depends only on these counts:

$$\pi_e = \sum_{a<b\in[K]} \#^e_a \#^e_b \, p_{ab} + \sum_{a\in[K]} \frac{\#^e_a(\#^e_a - 1)}{2} \, p_{aa} . \tag{E1}$$

Hence, all hyperedges with different nodes, but same counts $\#^e_1, \ldots, \#^e_K$, have equal probability. With this in mind, we sample hypergraphs following these steps.

1. Iterate over the combinations.
   For hyperedge size $d = 2$, we can sample all the $N(N-1)/2$ edges directly. Otherwise, iterate the following procedure for every other hyperedge size $d = 3, \ldots, D$ and vectors $\# = (\#_1, \ldots, \#_K)$ of community counts (independent of e to highlight that same counts yield identical Eq. (E1)) satisfying $\sum_{a=1}^{K} \#_a = d$.

2. Compute the probability.
   For a given count vector $\#$, the resulting hyperedge probability $\pi_\#$ is given in Eq. (E1). Also notice that there are $N_\# = \binom{N_1}{\#_1} \cdot \ldots \cdot \binom{N_K}{\#_K}$ possible hyperedges satisfying the count $\#$, since we can choose $\#_1$ nodes from the N_1 nodes in community 1, $\#_2$ out of N_2, and so on.

3. Sample the number of hyperedges.
   The key idea is not to sample the individual hyperedges, but the *number* of observed hyperedges. Since the individual hyperedges are independent Bernoulli variables with same probability, their sum X follows a binomial distribution:

$$X \sim \text{Binom}\left(N_\#, \frac{\pi_\#}{\kappa_d}\right) \tag{E2}$$

   with probability $\pi_\#$ fixed, determined by $\#$, and number of realizations $N_\#$. Sampling directly from Eq. (E2) is numerically challenging for large $N_\#$ and κ_d, hence we adopt a Gaussian approximation for the binomial [62]. Similarly, we find a Poisson approximation to be more stable for large $N_\#$ and small $\pi_\#/\kappa_d$ [63]. We also adopt a Ramanujan approximation for large log-factorials appearing during the calculations [64]. This substantially speeds up sampling, while being extremely precise.

4. Sample the final hyperedges.
   Given the count X of hyperedges, sampled from Eq. (E2), we can sample the hyperedges. This operation is performed by independently sampling X times $\#_1$ nodes from community 1, $\#_2$ from community 2, and so on. As an important point, notice that this procedure might yield repeated hyperedges, which are not allowed. In sparse regimes, this event has low probability [65]. As a sensible approximation, one can simply proceed by deleting repetitions, or resample single hyperedges until the desired number X of distinct realizations is reached. In our experiments, we choose the former option. Our code implementation [42] has both choices available for practitioners.

2. Computational complexity

For a fixed hyperedge size d, there are two parts to the computational cost: iterating through the counts $\#$, and sampling the hyperedges. The number of counts is fixed and given by $K^d/d!$, i.e., the number of possible ways to assign d nodes to K groups, without order. The cost of sampling the hyperedges can be precisely quantified since every d-dimensional hyperedge has a cost d, and there is an average number k_d of such hyperedges. Calling Ω^d the space of all d-dimensional hyperedges, we find

$$
\begin{aligned}
\mathbb{E}[k_d] &= \sum_{e\in\Omega^d} \mathbb{P}(e \,|\, p, t) \\
&= \sum_{e\in\Omega^d} \sum_{i<j\in e} \frac{p_{t_i t_j}}{\kappa_d} \\
&= \frac{1}{\kappa_d} \sum_{e\in\Omega^d} \sum_{i<j\in e} p_{t_i t_j} \\
&= \frac{\binom{N-2}{d-2}}{\kappa_d} \sum_{i<j\in V} p_{t_i t_j} \\
&\approx \frac{\binom{N-2}{d-2} N^2}{\kappa_d} \sum_{b\leq d=1}^{K} p_{bd} n_b n_d .
\end{aligned} \tag{E3}
$$

Hence, the average computational cost is given by

$$\sum_{d=2}^{D} O\left(\frac{K^d}{d!} + d\,\mathbb{E}[k_d]\right) . \tag{E4}$$

Given the large size of Ω^d, the cost in Eq. (E4) tightly concentrates around the expected value. In sparse regimes, the term $K^d/d!$ dominates, as the number of hyperedges k_d is low, while the two terms both contribute to the cost when $\mathbb{E}[k_d]$ grows.

3. Experiments

We employ the sampling algorithm to generate the hypergraphs used to study the phase transition of Sec. IV B. Here, we set the affinity matrix to have all equal in-degree $c_{aa} = c_{in}$ and out-degree $c_{ab} = c_{out}$, so that Eq. (15) becomes $c_{in} + (K-1)c_{out} = Kc$ for some K and c. In our experiments, we sample hypergraphs with $N = 10^4$ nodes by fixing $c = 10$ and $K = 4$, we span across 65 values of c_{out} in $[0, 500]$, and compute the corresponding $c_{in} = c_{in}(c_{out}; K, c)$. For each experimental configuration c_{in}, c_{out}, we draw 5 hypergraphs from different random seeds. This gives a total of 325 hypergraphs.

We use the expected number of d-dimensional hyperedges $\mathbb{E}[k_d]$ in Eq. (E4) and the average degree $\langle d \rangle$ in Eq. (A2) to perform a sanity check between our sampling algorithm and theoretical derivations. For constant in and out-degree, these two metrics evaluate to

$$\mathbb{E}[k_d] \approx \frac{Nc}{d(d-1)} \quad ,$$

$$\langle d \rangle \approx \frac{Cc}{2} .$$

The results in Fig. 6 show excellent agreement between theory and experiments. We also highlight that the sampling method is extremely fast and has an average sampling time of $t = 32.7 \pm 2.7$ on the experimental setup considered here.
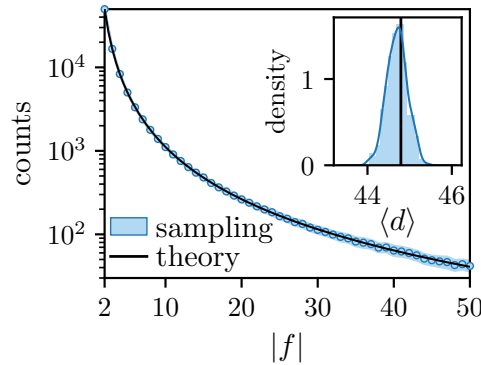

FIG. 6: **Sampling experiments.** The expected number of $|f|$-dimensional hyperedges returned by our experiments (blue) is in great accordance with the theoretical prediction $\mathbb{E}[k_{|f|}]$ (black). Similarly, the experimental expected degrees distribute around the analytical $\langle d \rangle$. Shaded areas are standard deviations over 5 random hypergraph extractions, at each $|f|$.

Appendix F: Phase transition: complementary derivations and additional results

1. Proof of Proposition 1

First, we want to prove that all communities have the same expected degree. In order to do that, we start by computing the expected degree $\langle d_i \rangle$ of a given node $i \in V$. Following similar derivations to those for $\langle d \rangle$ Appendix A, we find

$$
\begin{aligned}
\langle d_i \rangle &= \sum_{e \in E: i \in e} \mathbb{P}(e \mid p, t) \\
&= \sum_{e \in E: i \in e} \frac{\pi_e}{\kappa_e} \\
&= C' \sum_{a=1}^{K} c_{t_i a} n_a + \frac{NC''}{2} \left(\sum_{b,d=1}^{K} c_{bd} n_b n_d + \sum_{b=1}^{K} c_{bb} n_b^2 \right),
\end{aligned}
$$

where $C' = \sum_{d=2}^{D} \binom{N-2}{d-2}/\kappa_d$, as previously defined, and $C'' = \sum_{d=3}^{D} \binom{N-3}{d-3}/\kappa_d$. Therefore, the average degree $\langle b \rangle$ of a community $b \in [K]$, evaluates to

$$
\begin{aligned}
\langle b \rangle &= \frac{1}{N_b} \sum_{i \in V: t_i = b} \langle d_i \rangle \\
&= \frac{1}{N_b} \sum_{i \in V: t_i = b} \left[C' \sum_{a=1}^{K} c_{t_i a} n_a + \frac{NC''}{2} \left(\sum_{d,m=1}^{K} c_{dm} n_d n_m + \sum_{d=1}^{K} c_{dd} n_d^2 \right) \right] \\
&= \frac{1}{N_b} \sum_{i \in V: t_i = b} \left[C' \sum_{a=1}^{K} c_{ba} n_a + \frac{NC''}{2} \left(\sum_{d,m=1}^{K} c_{dm} n_d n_m + \sum_{d=1}^{K} c_{dd} n_d^2 \right) \right] \\
&= C' \sum_{a=1}^{K} c_{ba} n_a + \frac{NC''}{2} \left(\sum_{d,m=1}^{K} c_{dm} n_d n_m + \sum_{d=1}^{K} c_{dd} n_d^2 \right) \\
&= C' c + \frac{NC''}{2} \left(\sum_{d,m=1}^{K} c_{dm} n_d n_m + \sum_{d=1}^{K} c_{dd} n_d^2 \right),
\end{aligned}
$$

which is independent of the specific choice of group b, from which we conclude that all the groups yield equal expected degrees.

Second, we wish to demonstrate that MP's fixed points are as in Eqs. (16)–(17). Notice that in the derivations here below, when convenient, we interchange equivalent summations over function nodes' neighbors ∂e and hyperedge e. By treating all quantities

that are independent of t_i in $q_{i \to e}(t_i), \widehat{q}_{e \to i}(t_i)$ as a constant, we evaluate Eq. (7) as

$$
\begin{aligned}
\widehat{q}_{e \to i}(t_i) &\propto \sum_{t_j : j \in e \setminus i} \frac{\pi_e}{\kappa_e} \prod_{j \in \partial e \setminus i} q_{j \to e}(t_j) \\
&\propto \sum_{t_j : j \in e \setminus i} \sum_{r < s \in e} p_{t_r t_s} \prod_{j \in \partial e \setminus i} q_{j \to e}(t_j) \\
&= \sum_{t_j : j \in e \setminus i} \left(\sum_{r \in e \setminus i} p_{t_r t_i} \prod_{j \in \partial e \setminus i} q_{j \to e}(t_j) + \sum_{r < s \in e \setminus i} p_{t_r t_s} \prod_{j \in \partial e \setminus i} q_{j \to e}(t_j) \right) \\
&= \sum_{r \in e \setminus i} \sum_{t_r} p_{t_r t_i} q_{r \to e}(t_r) + \sum_{r < s \in e \setminus i} \sum_{t_r, t_s} p_{t_r t_s} q_{r \to e}(t_r) q_{s \to e}(t_s) \\
&= \sum_{r \in e \setminus i} \sum_{t_r} p_{t_r t_i} n_{t_r} + \sum_{r < s \in e \setminus i} \sum_{t_r, t_s} p_{t_r t_s} n_{t_r} n_{t_s} \\
&= \frac{1}{N} \left(\sum_{r \in e \setminus i} c + \sum_{r < s \in e \setminus i} c \right) \\
&= \frac{c}{N} \left((|e| - 1) + c \frac{|e|(|e| - 1)}{2} \right) .
\end{aligned}
\tag{F1}
$$

Since messages $\widehat{q}_{e \to i}(t_i)$ are normalized to have unitary sum, Eq. (F1) implies that $\widehat{q}_{e \to i}(t_i) = 1/K$. Substituting this result into Eq. (8), one finds also that $q_i(t_i) = n_{t_i}$. The variable-to-function node messages are updated with Eq. (9), which includes Eq. (12) for the external field $h(t_i)$. The external field evaluated at fixed points is also constant, in fact

$$
\begin{aligned}
h(t_i) &= \frac{C'}{N} \sum_{j \in V} \sum_{t_j} c_{t_i t_j} q_j(t_j) \\
&= \frac{C'}{N} \sum_{j \in V} \sum_{t_j} c_{t_i t_j} n_{t_j} \\
&= \frac{C'}{N} \sum_{j \in V} c \\
&= C' c .
\end{aligned}
\tag{F2}
$$

The result of Eq. (F2) implies that the messages in Eq. (9) read

$$q_{i \to e}(t_i) \propto n_{t_i} \left(\prod_{\substack{f \in E \\ f \in \partial i \backslash e}} \sum_{t_j : j \in \partial f \backslash i} \pi_f \prod_{j \in \partial f \backslash i} q_{j \to f}(t_j) \right)$$

$$= n_{t_i} \left(\prod_{\substack{f \in E \\ f \in \partial i \backslash e}} \sum_{t_j : j \in \partial f \backslash i} \pi_f \prod_{j \in \partial f \backslash i} n_{t_j} \right)$$

$$\propto n_{t_i} \left(\prod_{\substack{f \in E \\ f \in \partial i \backslash e}} \sum_{r < s \in f} \sum_{t_j : j \in \partial f \backslash i} p_{t_r t_s} \prod_{j \in \partial f \backslash i} n_{t_j} \right)$$

$$\propto n_{t_i} \left[\prod_{\substack{f \in E \\ f \in \partial i \backslash e}} \left(\sum_{r < s \in f} \sum_{t_r t_s} p_{t_r t_s} n_{t_r} n_{t_s} + \sum_{r \in f \backslash i} \sum_{t_r} p_{t_r t_i} n_{t_r} \right) \right]$$

$$\propto n_{t_i} \left[\prod_{\substack{f \in E \\ f \in \partial i \backslash e}} \left(\frac{|f|(|f|-1)}{2} c + (|f|-1)c \right) \right]$$

$$\propto n_{t_i} ,$$

which is exactly Eq. (17).

2. Transition matrix formula

In this section, we derive the expression for the transition matrix $\tilde{T}_r^{ab}$ in Eq. (19). To simplify the notation, we indicate the (variable node, function node) pairs at level r as $(i_r, f_r) = (i, e)$, and similarly, at level $r + 1$ we use $(i_{r+1}, f_{r+1}) = (j, f)$. Hence, the transition matrix becomes

$$\tilde{T}_r^{ab} = \frac{\partial q_{i \to e}(a)}{\partial q_{j \to f}(b)} .$$

In order to find a closed-form expression of $\tilde{T}_r^{ab}$, we claim that the two following Lemmas hold.

Lemma 1. *Under the constant group degree assumption in Eq. (15):*

   1. for any hyperedge e and nodes $i \in e$:

$$\sum_{t_j : j \in e \backslash i} \pi_e \prod_{k \in e \backslash i} q_{k \to e}(t_k) = \frac{c|e|(|e|-1)}{2N} ; \tag{F3}$$

   2. for any hyperedge e and nodes $i, j \in e$:

$$\sum_{t_k : k \in e \backslash i, j} \pi_e \prod_{m \in e \backslash i, f} q_{m \to e}(t_m) = \frac{1}{N} \left[c_{t_i t_j} + c(|e|-2) \left(2 + \frac{|e|-3}{2} \right) \right] . \tag{F4}$$

Lemma 2 (Employing Lemma 1). *Under the constant group degree assumption in Eq. (15):*

   1. the derivative $\partial \exp(-h(a))/\partial q_{i \to e}(b)$ is negligible to leading order in N;

   2. the external field is constant $h(t_i) = $ const.;

3. call $Z^{i \to e}$ the normalizing constant of $q_{i \to e}$, then

$$Z^{i \to e} = \prod_{g \in \partial i \backslash e} c^{\frac{|g|(|g|-1)}{2N}} \tag{F5}$$

$$\frac{\partial Z^{i \to e}}{\partial q_{j \to f}(b)} = \frac{c}{N} \left(\prod_{g \in \partial i \backslash e, f} c^{\frac{|g|(|g|-1)}{2N}} \right) \left[1 + (|f|-2)\left(2 + \frac{|f|-3}{2}\right) \right] . \tag{F6}$$

The claims allow us to derive the transition matrix. Particularly, we make explicit all derivatives and variable-to-function nodes messages as in Eq. (9). By also ignoring all terms relative to $h(t_i)$ thanks to Lemma 2, we get

$$\frac{\partial q_{i \to e}(a)}{\partial q_{j \to f}(b)} \approx -\frac{1}{(Z^{i \to e})^2} \frac{\partial Z^{i \to e}}{\partial q_{j \to f}(b)} n_{t_i} \left(\prod_{g \in \partial i \backslash e} \sum_{t_m : m \in \partial g \backslash i} \pi_g \prod_{m \in \partial g \backslash i} q_{m \to g}(t_m) \right)$$

$$+ \frac{1}{Z^{i \to e}} n_{t_i} \left(\prod_{g \in \partial i \backslash e, f} \sum_{t_m : m \in \partial g \backslash i} \pi_g \prod_{m \in \partial g \backslash i} q_{m \to g}(t_m) \right) \left(\sum_{t_m : m \in \partial f \backslash i, j} \pi_f \prod_{m \in \partial f \backslash i, j} q_{m \to f}(t_m) \right) .$$

The terms involving $Z^{i \to e}$ are in Lemma 2 (Eq. (F5) and Eq. (F6)), while the expressions in parentheses are in Lemma 1 (Eq. (F3) and Eq. (F4)). By performing all the substitutions we get

$$\frac{\partial q_{i \to e}(a)}{\partial q_{j \to f}(b)} = \tag{F7}$$

$$- n_{t_i} \left(\prod_{g \in \partial i \backslash e} c^{\frac{|g|(|g|-1)}{2N}} \right)^{-2} \left(\prod_{g \in \partial i \backslash e, f} c^{\frac{|g|(|g|-1)}{2N}} \right) \left(\prod_{g \in \partial i \backslash e} c^{\frac{|g|(|g|-1)}{2N}} \right) \frac{c}{N} \left[1 + (|f|-2)\left(2 + \frac{|f|-3}{2}\right) \right]$$

$$+ n_{t_i} \left(\prod_{g \in \partial i \backslash e} c^{\frac{|g|(|g|-1)}{2N}} \right)^{-1} \left(\prod_{g \in \partial i \backslash e, f} c^{\frac{|g|(|g|-1)}{2N}} \right) \frac{1}{N} \left[c_{t_i t_j} + c(|f|-2)\left(2 + \frac{|f|-3}{2}\right) \right]$$

$$= n_{t_i} \left(c^{\frac{|f|(|f|-1)}{2N}} \right)^{-1} \left\{ -\frac{c}{N} \left[1 + (|f|-2)\left(2 + \frac{|f|-3}{2}\right) \right] + \frac{1}{N} \left[c_{t_i t_j} + c(|f|-2)\left(2 + \frac{|f|-3}{2}\right) \right] \right\}$$

$$= \frac{2}{|f|(|f|-1)} n_{t_i} \left(\frac{c_{t_i t_j}}{c} - 1 \right)$$

$$= \frac{2}{|f|(|f|-1)} n_a \left(\frac{c_{ab}}{c} - 1 \right)$$

which is exactly the expression in Eq. (19).

What is left to complete all derivations is to prove Lemma 1 and Lemma 2, which is done next.

a. Proof of Lemma 1

1. Derivation of Eq. (F3):

$$\sum_{t_j : j \in e \backslash i} \pi_e \prod_{k \in e \backslash i} q_{k \to e}(t_k) = \sum_{t_j : j \in e \backslash i} \sum_{r < s \in e} p_{t_r t_s} \prod_{k \in e \backslash i} q_{k \to e}(t_k)$$

$$= \sum_{r < s \in e \backslash i} \sum_{t_r t_s} p_{t_r t_s} q_{r \to e}(t_r) q_{s \to e}(t_s) + \sum_{r \in e \backslash i} \sum_{t_r} p_{t_r t_i} q_{r \to e}(t_r)$$

$$= \frac{1}{N} \sum_{r < s \in e \backslash i} \sum_{t_r, t_s} c_{t_r t_s} n_{t_r} n_{t_s} + \frac{1}{N} \sum_{r \in e \backslash i} \sum_{t_r} c_{t_r t_i} n_{t_r}$$

$$= \frac{c}{N} \left[\frac{(|e|-1)(|e|-2)}{2} + (|e|-1) \right]$$

$$= \frac{c(|e|-1)|e|}{2N} .$$

2. Derivation of Eq. (F4):

$$
\sum_{t_k:k\in e\setminus i,j} \pi_e \prod_{m\in e\setminus i,j} q_{m\to e}(t_m) = \sum_{t_k:k\in e\setminus i,j} \sum_{r<s\in e} p_{t_r t_s} \prod_{m\in e\setminus i,j} q_{m\to e}(t_m)
$$

$$
= p_{t_i t_j} + \sum_{r\in e\setminus i,j} \sum_{t_r} p_{t_r t_i} q_{r\to e}(t_r) + \sum_{r\in e\setminus i,j} \sum_{t_r} p_{t_r t_j} q_{r\to e}(t_r)
$$

$$
+ \sum_{r<s\in e\setminus i,j} \sum_{t_r,t_s} p_{t_r t_s} q_{r\to e}(t_r) q_{s\to e}(t_s)
$$

$$
= \frac{1}{N}\left(c_{t_i t_j} + \sum_{r\in e\setminus i,j}\sum_{t_r} c_{t_r t_i} n_{t_r} + \sum_{r\in e\setminus i,j}\sum_{t_r} c_{t_r t_j} n_{t_r} + \sum_{r<s\in e\setminus i,j}\sum_{t_r,t_s} c_{t_r t_s} n_{t_r} n_{t_s} \right)
$$

$$
= \frac{1}{N}\left(c_{t_i t_j} + \sum_{r\in e\setminus i,j} c + \sum_{r\in e\setminus i,j} c + \sum_{r<s\in e\setminus i,j} c \right)
$$

$$
= \frac{1}{N}\left[c_{t_i t_j} + c(|e|-2)\left(2 + \frac{|e|-3}{2}\right)\right].
$$

b. Proof of Lemma 2

1. Using Eq. (12), we write

$$
\frac{\partial \exp(-h(a))}{\partial q_{i\to e}(b)} = \exp\left(-\frac{C'}{N}\sum_{v\in V}\sum_{t_k} c_{at_k} q_k(t_k)\right)\left(-\frac{C'}{N}\sum_{k\in V}\sum_{t_v} c_{at_k}\frac{\partial q_k(t_k)}{\partial q_{i\to e}(b)}\right). \tag{F8}
$$

Only few of the derivatives $\partial q_k(t_k)/\partial q_{i\to e}(b)$ entering Eq. (F8) are non-zero. Hence, the full derivative has negligible order $O(1/N)$.

2. The fact that the external field is constant was already shown in Eq. (F2) during the proof of Proposition 1.

3. As just proved, we can ignore the external field in the expression of $Z^{i\to e}$, and find

$$
Z^{i\to e} \approx \sum_{t_i} q_{i\to e}(t_i)
$$

$$
= \sum_{t_i} n_{t_i}\left(\prod_{g\in\partial i\setminus e}\sum_{t_j:j\in\partial g\setminus i}\pi_g\prod_{j\in\partial g\setminus i} q_{j\to g}(t_j)\right). \tag{F9}
$$

Utilizing result Eq. (F3) in Lemma 1, Eq. (F9) simplifies to

$$
Z^{i\to e} = \sum_{t_i} n_{t_i}\left(\prod_{g\in\partial i\setminus e} c\frac{|g|(|g|-1)}{2N}\right)
$$

$$
= \left(\prod_{g\in\partial i\setminus e} c\frac{|g|(|g|-1)}{2N}\right).
$$

which results in Eq. (F5), as desired. Similarly, to compute the derivative $\partial Z^{i\to e}/\partial q_{j\to f}(b)$ we can ignore all appearing $\partial \exp(-h(a))/\partial q_{j\to f}(b)$ and $h(t_i)$ thanks the Lemma's first two points (just proved). Hence

$$
\frac{\partial Z^{i\to e}}{\partial q_{j\to f}(b)} = \frac{\partial}{\partial q_{j\to f}(b)}\left[\sum_{t_i} n_{t_i}\left(\prod_{g\in\partial i\setminus e}\sum_{t_j:j\in\partial g\setminus i}\pi_g\prod_{j\in\partial g\setminus i} q_{j\to g}(t_j)\right)\right]
$$

$$
= \sum_{t_i} n_{t_i}\left(\prod_{g\in\partial i\setminus e,f}\sum_{t_m:m\in\partial g\setminus i}\pi_g\prod_{m\in\partial g\setminus i} q_{m\to g}(t_m)\right)\left(\sum_{t_m:m\in\partial f\setminus i,j}\pi_f\prod_{m\in\partial f\setminus i,j} q_{m\to f}(t_m)\right),
$$

and using Eq. (F3) and Eq. (F4) from Lemma 1, conclude with

$$= \frac{1}{N} \left(\prod_{g \in \partial i \backslash e, f} c^{\frac{|g|(|g|-1)}{2N}} \right) \left[\sum_{t_i} n_{t_i} c_{t_i t_j} + c(|f|-2) \left(2 + \frac{|f|-3}{2} \right) \right]$$

$$= \frac{c}{N} \left(\prod_{g \in \partial i \backslash e, f} c^{\frac{|g|(|g|-1)}{2N}} \right) \left[1 + (|f|-2) \left(2 + \frac{|f|-3}{2} \right) \right] .$$

3. Elapsed time of MP

In Fig. 7, we plot the running time of MP when performing the synthetic experiments of Sec. IV B. Elapsed times become prohibitively large when $c_{\text{out}}/c_{\text{in}}$ increases. For this reason, we threshold the maximum number of MP iterations and obtain the plateaus of Fig. 7.
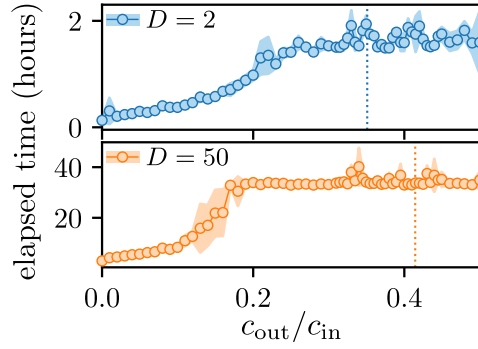

FIG. 7: **Elapsed time for MP.** For both $D = 2$ and $D = 5$, the elapsed times plateau due to the threshold imposed on MP's maximum number of iterations. Shaded areas are standard deviations over 5 random initializations of MP. Vertical dotted lines are theoretical detectability bounds derived from Eq. (26).

Appendix G: Calculations of the free energy

After MP, it is possible to approximate the log-evidence of the data, i.e., the log-normalizing constant $\log Z$, as per Eq. (5). The equivalent quantity $F = -\log Z$, called the free energy of the system, can be obtained via the following cavity-based general formula:

$$F \approx -\sum_{i \in V} f_i + \sum_{e \in \Omega} (|e|-1) f_e , \tag{G1}$$

where

$$f_i = \log \left(\sum_{t_i} n_{t_i} \prod_{e \in \partial i} \sum_{t_j : j \in \partial e \backslash i} \left(\frac{\pi_e}{\kappa_e} \right)^{A_e} \left(1 - \frac{\pi_e}{\kappa_e} \right)^{1 - A_e} \prod_{j \in \partial e \backslash i} q_{j \to e}(t_j) \right)$$

$$f_e = \log \left(\sum_{t_j : j \in \partial e} \left(\frac{\pi_e}{\kappa_e} \right)^{A_e} \left(1 - \frac{\pi_e}{\kappa_e} \right)^{1 - A_e} \prod_{j \in \partial e} q_{j \to e}(t_j) \right) .$$

Assuming that MP has converged, all messages $q_{j \to e}(t_j)$ are available. Notice, however, that naive computations of the f_i and f_e addends are unfeasible, due to the exploding sums over $t_j : j \in \partial e$. In the following, we show how such computations can be performed efficiently.

1. Calculations of f_i.

As one can observe from Eq. (B1) and Eq. (B2), the f_i terms are the log-normalizing constants of q_i, therefore they can be computed similarly. In particular, ignoring constants, by Eq. (B13), the following simplification holds:

$$f_i = \log \left(\sum_{t_i} n_{t_i} \prod_{\substack{e \in E \\ e \in \partial i}} \sum_{t_j : j \in \partial e \setminus i} \pi_e \prod_{j \in \partial e \setminus i} q_{j \to e}(t_j) \exp(-h(t_i)) \right).$$

The single terms indexed by $e \in E$, i.e., the values $\sum_{t_j : j \in \partial e \setminus i} \pi_e \prod_{j \in \partial e \setminus i} q_{j \to e}(t_j)$, are equivalent to the unnormalized messages $\widehat{q}_{e \to j}(t_j)$. For this reason, they can be computed with the same dynamic program presented in Appendix D 1.

2. Calculations of f_e.

While the f_i terms in Eq. (G1) are computed singularly, we take a different approach and calculate the whole sum $\sum_{e \in \Omega}(|e|-1)f_e$ without computing the single f_e, as this would be impossible due to their exploding number. First, we separate the terms over Ω in Eq. (G1) as follows.

$$\sum_{e \in \Omega}(|e|-1)f_e = \sum_{e \in \Omega}(|e|-1)\log \left(\sum_{t_j : j \in \partial e} \left(\frac{\pi_e}{\kappa_e}\right)^{A_e} \left(1 - \frac{\pi_e}{\kappa_e}\right)^{1-A_e} \prod_{j \in \partial e} q_{j \to e}(t_j) \right)$$

$$= \log \left(\prod_{e \in \Omega} \left[\sum_{t_j : j \in \partial e} \left(\frac{\pi_e}{\kappa_e}\right)^{A_e} \left(1 - \frac{\pi_e}{\kappa_e}\right)^{1-A_e} \prod_{j \in \partial e} q_{j \to e}(t_j) \right]^{|e|-1} \right)$$

$$= \log \left(\prod_{e \in E} \left[\sum_{t_j : j \in \partial e} \pi_e \prod_{j \in \partial e} q_{j \to e}(t_j) \right]^{|e|-1} \right) + \log \left(\prod_{e \in \Omega \setminus E} \left[\sum_{t_j : j \in \partial e} \left(1 - \frac{\pi_e}{\kappa_e}\right) \prod_{j \in \partial e} q_{j \to e}(t_j) \right]^{|e|-1} \right) + \text{const.}.$$

This allows us to compute the last two addends separately.

Focusing on the second addend, and proceeding similarly as for the external field calculations that brought to Eq. (B19), we get

$$\log \prod_{e \in \Omega \setminus E} \left[\sum_{t_j : j \in \partial e} \left(1 - \frac{\pi_e}{\kappa_e}\right) \prod_{j \in \partial e} q_{j \to e}(t_j) \right]^{|e|-1} \approx \log \prod_{e \in \Omega \setminus E} \left[\exp\left(-\frac{1}{N} \sum_{t_j : j \in \partial e} \left(\frac{\sum_{k < m \in e} c_{t_k t_m}}{\kappa_e}\right) \prod_{j \in \partial e} q_{j \to e}(t_j) \right) \right]^{|e|-1}$$

$$\approx \log \prod_{e \in \Omega \setminus E} \left[\exp\left(-\frac{1}{N} \sum_{t_j : j \in \partial e} \left(\frac{\sum_{k < m \in e} c_{t_k t_m}}{\kappa_e}\right) \prod_{j \in \partial e} q_j(t_j) \right) \right]^{|e|-1}$$

$$= \log \prod_{e \in \Omega \setminus E} \exp\left(\frac{1 - |e|}{N} \sum_{t_j : j \in \partial e} \left(\frac{\sum_{k < m \in e} c_{t_k t_m}}{\kappa_e}\right) \prod_{j \in \partial e} q_j(t_j) \right)$$

$$\approx \log \prod_{e \in \Omega} \exp\left(\frac{1 - |e|}{N} \sum_{t_j : j \in \partial e} \left(\frac{\sum_{k < m \in e} c_{t_k t_m}}{\kappa_e}\right) \prod_{j \in \partial e} q_j(t_j) \right)$$

$$= \sum_{e \in \Omega} \frac{1 - |e|}{N} \sum_{t_j : j \in \partial e} \left(\frac{\sum_{k < m \in e} c_{t_k t_m}}{\kappa_e}\right) \prod_{j \in \partial e} q_j(t_j)$$

$$= \frac{1}{N} \sum_{e \in \Omega} \frac{1 - |e|}{\kappa_e} \sum_{k < m \in e} \sum_{t_j : j \in \partial e} c_{t_k t_m} \prod_{j \in \partial e} q_j(t_j)$$

$$= \frac{1}{N} \sum_{e \in \Omega} \frac{1 - |e|}{\kappa_e} \sum_{k < m \in e} \sum_{t_k t_m} c_{t_k t_m} q_k(t_k) q_j(t_j)$$

$$= \frac{C'''}{N} \sum_{k < m \in V} \sum_{t_k t_m} c_{t_k t_m} q_k(t_k) q_j(t_j)$$

where $C''' := \sum_{d=2}^{D} \frac{1-d}{\kappa_d} \binom{N-2}{d-2}$. Also define $q_V(a) = \sum_{k \in V} q_k(a)$. Then,

$$
\log \prod_{e \in \Omega \setminus E} \left[\sum_{t_j : j \in \partial e} \left(1 - \frac{\pi_e}{\kappa_e} \right) \prod_{j \in \partial e} q_{j \to e}(t_j) \right]^{|e|-1} \approx \frac{C'''}{N} \sum_{k < m \in V} \sum_{t_k t_m} c_{t_k t_m} q_k(t_k) q_j(t_j)
$$

$$
= \frac{C'''}{N} \sum_{ab} c_{ab} \sum_{k < m \in V} q_k(a) q_j(b)
$$

$$
= \frac{C'''}{2N} \sum_{ab} c_{ab} \left[\sum_{k,m \in V} q_k(a) q_j(b) - \sum_{k \in V} q_k(a) q_k(b) \right]
$$

$$
= \frac{C'''}{2N} \sum_{ab} c_{ab} \left[q_V(a) q_V(b) - \sum_{k \in V} q_k(a) q_k(b) \right]
$$

which can be computed in linear time $O(|V| K^2)$.

The first addend requires different considerations. Since naive calculations of every sum on $t_j : j \in \partial e$ cost $O(K^{|e|})$, and thus are unfeasible, we design a dynamic program similar to that of Appendix D 1. For simplicity, consider a hyperedge $e = 1, \ldots, m$. Proceeding as in Appendix D 1, we define the quantities:

$$
\tilde{\eta}(e, n) = \sum_{t_j : j = 1, \ldots, n} \pi_e \prod_{j = 1, \ldots, n} q_{j \to e}(t_j) \tag{G2}
$$

$$
\tilde{s}_n(a) = \sum_{t_1} p_{a t_1} q_{1 \to e}(t_1) + \ldots + \sum_{t_{n-1}} p_{a t_{n-1}} q_{n-1 \to e}(t_{n-1}). \tag{G3}
$$

Notice that $\tilde{\eta}(e, m) = \sum_{t_j : j \in \partial e} \pi_e \prod_{j : j \in \partial e} q_{j \to e}(t_j)$ is the quantity we need to compute. For Eqs. (G2)–(G3), the following recursions hold:

$$
\tilde{\eta}(e, n) = \tilde{\eta}(e, n - 1) + \sum_{t_n} q_{n \to e}(t_n) \tilde{s}_n(t_n)
$$

$$
\tilde{s}_n(a) = \tilde{s}_{n-1}(a) + \sum_{t_{n-1}} p_{t_{n-1} a} q_{n-1 \to e}(t_{n-1}).
$$

Here, computing the final $\tilde{\eta}(e, m)$ costs $O(K|e|)$, and computing it for all the observed hyperedges costs $\sum_{e \in E} O(K|e|)$. Notice that utilizing the dynamic program in Appendix D 1 would cost $\sum_{e \in E} O(K^2 |e|^2)$, plus the processing needed to obtain the $\tilde{\eta}(e, m)$ value. Hence, the new recursions result in good computing savings with minimal changes to the numerical implementation.

1. Computation of the free energy landscape on High School data

We explain further how to obtain the free energy landscape of the High School dataset in Fig. 5. The three vertices are inferred using the dataset's hyperedges whose size is lower or equal than D, with $D = 2, 3, 4$. After having performed inference on every vertex, we obtain the parameters $(p_2, n_2), (p_3, n_3), (p_4, n_4)$—each pair is associated with a value of D—for the affinity matrix and the community prior.

Every point in the simplex is generated with a convex combination of the three vertices. Particularly, we define the parameters

$$
p_{\text{simplex}} = \lambda_2 p_2 + \lambda_3 p_3 + \lambda_4 p_4
$$

$$
n_{\text{simplex}} = \lambda_2 n_2 + \lambda_3 n_3 + \lambda_4 n_4,
$$

where $0 \le \lambda_i \le 1$ and $\sum_{i=2,3,4} \lambda_i = 1$. For any value of $p_{\text{simplex}}, n_{\text{simplex}}$, we compute the free energy on the whole High School dataset, i.e., taking all hyperedges. The free energy approximations following Eq. (G1) require the messages, marginals and external field, which can be inferred via MP and in turn depend on $p_{\text{simplex}}, n_{\text{simplex}}$. For every point in the simplex, we fix $p_{\text{simplex}}, n_{\text{simplex}}$ and infer all the remaining quantities via MP, to then compute the free energy displayed in Fig. 5.
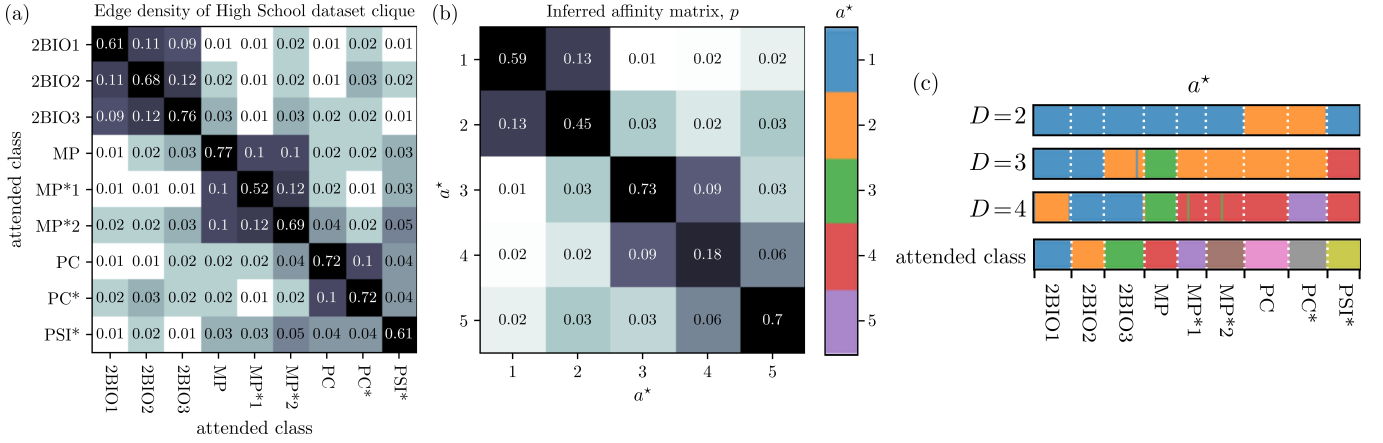
FIG. 8: **Affinity patterns on the High School dataset.** Colors of the matrices' entries are corresponding to their log values, properly normalized to ease the Figure's readability. **(a)** Edge density on the clique decomposition of the High School dataset. As in Mastrandrea *et al.* [57], the edge density between two classes X and Y corresponds to the number of observed edges between nodes of the classes, normalized with respect to the total number of possible edges between X and Y. **(b)** Affinity matrix p inferred by the EM-MP scheme with $D = 4$. The method detects 5 classes, whose affinity values are as in the matrix's entries. Colors of classes follow the color coding of Fig. 5(c). **(c)** Inferred communities of nodes and the partition in the classes of students. The panel is identical to Fig. 5(c).

2. Inference of class affinity on High School data

We expand on the community patterns detected on the High School data for $D = 4$, which are represented in Fig. 5. The nine classes observed in the data are named after their subjects of focus, and are: MP, MP*1, MP*2 (mathematics and physics), PC, PC* (physics and chemistry), PSI* (engineering), 2BIO1, 2BIO2, 2BIO3 (biology) [57].

We compare the the edge density patterns computed on the data in Mastrandrea *et al.* [57], and shown in Fig. 8(a), with the affinity matrix p inferred on the High School dataset fixing $D = 4$, shown in Fig. 8(b). Additionally, in Fig. 8(c), we plot the partition of the nodes into communities with their labeling in classes.

We observe that classes that are inferred in the same community appear to also belong to classes that have a larger number of external interactions with other classes in the same inferred community. For instance, the BIO classes belong to two communities that are disjoint from all others, see Fig. 8(c). Within the BIO classes, 2BIO2 and 2BIO3 are grouped in the same community, as they have slightly higher edge density of 0.12, compared to the 0.11 and 0.09 observed for 2BIO1.

The affinity matrix shown in Fig. 8(b) aligns well with the inter- and intra-community interactions. For instance, communities 1 and 2 (that contain the BIO classes) have an upper diagonal block that isolates them from all others. Communities 3 and 5, which largely match students from classes MP and PC, are disassortative with the remaining classes, grouped in community 4.

3. Further comments on higher-order interactions on High School data

D	AUC
2	0.710 ± 0.002
3	0.780 ± 0.003
4	0.843 ± 0.004
5	0.813 ± 0.003

TABLE I: **AUC scores on the High School dataset**. We perform MP and EM inference on the High School dataset utilizing hyperedges up to size D. Then, we compute the AUC on the full dataset, i.e. , on the hypergraph with all hyperedges up to $D = 5$. The goodness of link prediction, represented by the AUC score, shows that interactions up to size 4 improve the quality of inference, while utilizing interaction of size 5 yields a slight drop in performance.

The High School hypergraph contains interactions of orders ranging from 2 to 5. In our experiments, we observe that optimal inference is reached at maximum hyperedge size $D = 4$, while utilizing interactions of order 5 slightly degrades performance. We

confirm this in varioys ways. The communities inferred (now shown) are less granular than those presented for $D = 4$. A similar trend is observed in the free energy (not shown), that slightly increases when performing inference on the whole dataset. Finally, we measure the link prediction performances utilizing parameters inferred with $D = 2, 3, 4, 5$, and compute the AUC with respect to the full dataset, which we include in Table I. Here again we observe a slight drop in AUC when utilizing parameters inferred at $D = 5$, despite the AUC being computed with respect to all hyperedges, including those not observed when training on lower values of D.

There could be various reasons for this result. A possible explanation is that the interactions at $D = 5$ are noisier and/or less aligned with the data generating process assumed by our generative model. We recall that the data is collected via proximity sensors, and that social interactions in larger groups are harder to detect, and may arise from different types of link formation mechanisms.

REFERENCES

[1] M. Girvan and M. E. J. Newman, Community structure in social and biological networks, Proceedings of the National Academy of Sciences **99**, 7821 (2002).

[2] R. J. Fletcher, A. Revell, B. E. Reichert, W. M. Kitchens, J. D. Dixon, and J. D. Austin, Network modularity reveals critical scales for connectivity in ecology and evolution, Nature Communications **4**, 2572 (2013).

[3] M. E. J. Newman, The structure of scientific collaboration networks, Proceedings of the National Academy of Sciences **98**, 404 (2001).

[4] L. M. Shekhtman, S. Shai, and S. Havlin, Resilience of networks formed of interdependent modular networks, New Journal of Physics **17**, 123007 (2015).

[5] S. Fortunato, Community detection in graphs, Physics Reports **486**, 75 (2010).

[6] A. Decelle, F. Krzakala, C. Moore, and L. Zdeborová, Asymptotic analysis of the stochastic block model for modular networks and its algorithmic applications, Phys. Rev. E **84**, 066106 (2011).

[7] A. Decelle, F. Krzakala, C. Moore, and L. Zdeborová, Inference and Phase Transitions in the Detection of Modules in Sparse Networks, Phys. Rev. Lett. **107**, 065701 (2011).

[8] C. Moore, The Computer Science and Physics of Community Detection: Landscapes, Phase Transitions, and Hardness (2017), arXiv:1702.00467 [cs.CC].

[9] E. Abbe, Community Detection and Stochastic Block Models: Recent Developments, Journal of Machine Learning Research **18**, 1 (2018).

[10] A. Ghasemian, P. Zhang, A. Clauset, C. Moore, and L. Peel, Detectability Thresholds and Optimal Algorithms for Community Structure in Dynamic Networks, Phys. Rev. X **6**, 031005 (2016).

[11] D. Taylor, S. Shai, N. Stanley, and P. J. Mucha, Enhanced detectability of community structure in multilayer networks through layer aggregation, Phys. Rev. Lett. **116**, 228301 (2016).

[12] F. Battiston, G. Cencetti, I. Iacopini, V. Latora, M. Lucas, A. Patania, J.-G. Young, and G. Petri, Networks beyond pairwise interactions: Structure and dynamics, Physics Reports **874**, 1 (2020).

[13] F. Battiston, E. Amico, A. Barrat, G. Bianconi, G. Ferraz de Arruda, B. Franceschiello, I. Iacopini, S. Kéfi, V. Latora, Y. Moreno, M. M. Murray, T. P. Peixoto, F. Vaccarino, and G. Petri, The physics of higher-order interactions in complex systems, Nature Physics **17**, 1093 (2021).

[14] D. Zhou, J. Huang, and B. Schölkopf, Learning with Hypergraphs: Clustering, Classification, and Embedding, in Advances in Neural Information Processing Systems, Vol. 19, edited by B. Schölkopf, J. Platt, and T. Hoffman (MIT Press, 2006).

[15] P. S. Chodrow, N. Veldt, and A. R. Benson, Generative hypergraph clustering: From blockmodels to modularity, Science Advances **7**, eabh1303 (2021).

[16] M. Contisciani, F. Battiston, and C. De Bacco, Inference of hyperedges and overlapping communities in hypergraphs, Nature Communications **13**, 7229 (2022).

[17] N. Ruggeri, M. Contisciani, F. Battiston, and C. D. Bacco, Community detection in large hypergraphs, Science Advances **9**, eadg9159 (2023).

[18] I. Dumitriu and H. Wang, Exact recovery for the non-uniform Hypergraph Stochastic Block Model (2023), arXiv:2304.13139 [math.ST].

[19] M. C. Angelini, F. Caltagirone, F. Krzakala, and L. Zdeborová, Spectral detection on sparse hypergraphs, in 2015 53rd Annual Allerton Conference on Communication, Control, and Computing (Allerton) (2015) pp. 66–73.

[20] I. Chien, C.-Y. Lin, and I.-H. Wang, Community Detection in Hypergraphs: Optimal Statistical Limit and Efficient Algorithms, in Proceedings of the Twenty-First International Conference on Artificial Intelligence and Statistics, Proceedings of Machine Learning Research, Vol. 84, edited by A. Storkey and F. Perez-Cruz (PMLR, 2018) pp. 871–879.

[21] J. Liang, C. Ke, and J. Honorio, Information Theoretic Limits of Exact Recovery in Sub-hypergraph Models for Community Detection, in 2021 IEEE International Symposium on Information Theory (ISIT) (2021) pp. 2578–2583.

[22] S. Pal and Y. Zhu, Community detection in the sparse hypergraph stochastic block model, Random Structures & Algorithms **59**, 407 (2021).

[23] Q. Zhang and V. Y. F. Tan, Exact Recovery in the General Hypergraph Stochastic Block Model, IEEE Transactions on Information Theory **69**, 453 (2023).

[24] Y. Gu and Y. Polyanskiy, Weak recovery threshold for the hypergraph stochastic block model (2023), arXiv:2303.14689 [math.PR].

[25] S. Cole and Y. Zhu, Exact recovery in the hypergraph stochastic block model: A spectral algorithm, Linear Algebra and its Applications **593**, 45 (2020).

[26] C.-Y. Lin, I. E. Chien, and I.-H. Wang, On the fundamental statistical limit of community detection in random hypergraphs, in 2017 IEEE International Symposium on Information Theory (ISIT) (2017) pp. 2178–2182.

[27] D. Ghoshdastidar and A. Dukkipati, Consistency of Spectral Partitioning of Uniform Hypergraphs under Planted Partition Model, in Advances in Neural Information Processing Systems, Vol. 27, edited by Z. Ghahramani, M. Welling, C. Cortes, N. Lawrence, and K. Weinberger (Curran Associates, Inc., 2014).

[28] M. Yuan and Z. Shang, Information limits for detecting a subhypergraph, Stat **10**, e407 (2021).

[29] L. Corinzia, P. Penna, W. Szpankowski, and J. Buhmann, Statistical and computational thresholds for the planted k-densest sub-hypergraph problem, in Proceedings of The 25th Interna-

tional Conference on Artificial Intelligence and Statistics, Proceedings of Machine Learning Research, Vol. 151, edited by G. Camps-Valls, F. J. R. Ruiz, and I. Valera (PMLR, 2022) pp. 11615–11640.

[30] J. Jin, Z. T. Ke, and J. Liang, Sharp Impossibility Results for Hyper-graph Testing, in *Advances in Neural Information Processing Systems*, Vol. 34, edited by M. Ranzato, A. Beygelzimer, Y. Dauphin, P. Liang, and J. W. Vaughan (Curran Associates, Inc., 2021) pp. 7220–7231.

[31] M. Yuan, R. Liu, Y. Feng, and Z. Shang, Testing community structure for hypergraphs, The Annals of Statistics **50**, 147 (2022).

[32] P. Chodrow, N. Eikmeier, and J. Haddock, Nonbacktracking Spectral Clustering of Nonuniform Hypergraphs, SIAM Journal on Mathematics of Data Science **5**, 251 (2023).

[33] J. Pearl, Reverend Bayes on Inference Engines: A Distributed Hierarchical Approach, in *Proceedings of the Second AAAI Conference on Artificial Intelligence*, AAAI'82 (AAAI Press, 1982) p. 133–136.

[34] M. Mézard and A. Montanari, *Information, Physics, and Computation* (Oxford University Press, 2009).

[35] K. P. Murphy, *Machine learning: a probabilistic perspective* (MIT press, 2012).

[36] M. Mézard, G. Parisi, and M. Virasoro, *Spin Glass Theory and Beyond* (World Scientific, 1986).

[37] M. Mézard and G. Parisi, The bethe lattice spin glass revisited, The European Physical Journal B - Condensed Matter and Complex Systems **20**, 217 (2001).

[38] P. W. Holland, K. B. Laskey, and S. Leinhardt, Stochastic blockmodels: First steps, Social Networks **5**, 109 (1983).

[39] S. Wasserman and K. Faust, *Social Network Analysis: Methods and Applications*, Structural Analysis in the Social Sciences (Cambridge University Press, 1994).

[40] B. Kamiński, P. Prałat, and F. Théberge, Hypergraph Artificial Benchmark for Community Detection (h–ABCD), Journal of Complex Networks **11**, cnad028 (2023).

[41] N. Ruggeri, F. Battiston, and C. D. Bacco, A framework to generate hypergraphs with community structure (2023), arXiv:2212.08593 [cs.SI].

[42] N. Ruggeri, A. Lonardi, and C. De Bacco, Message-Passing on Hypergraphs: Detectability, Phase Transitions and Higher-Order Information, GitHub Repository, `https://github.com/nickruggeri/hypergraph-message-passing` (2023).

[43] G. T. Cantwell and M. E. J. Newman, Message passing on networks with loops, Proceedings of the National Academy of Sciences **116**, 23398 (2019).

[44] A. Kirkley, G. T. Cantwell, and M. E. J. Newman, Belief propagation for networks with loops, Science Advances **7**, eabf1211 (2021).

[45] A. P. Dempster, N. M. Laird, and D. B. Rubin, Maximum Likelihood from Incomplete Data via the EM Algorithm, Journal of the Royal Statistical Society. Series B (Methodological) **39**, 1 (1977), full publication date: 1977.

[46] H. Kesten and B. Stigum, Limit theorems for decomposable multi-dimensional Galton-Watson processes, Journal of Mathematical Analysis and Applications **17**, 309 (1967).

[47] H. Kesten and B. P. Stigum, Additional Limit Theorems for Indecomposable Multidimensional Galton-Watson Processes, The Annals of Mathematical Statistics **37**, 1463 (1966).

[48] M. Mézard and A. Montanari, Reconstruction on Trees and Spin Glass Transition, Journal of Statistical Physics **124**, 1317 (2006).

[49] E. Schneidman, M. J. Berry, R. Segev, and W. Bialek, Weak pairwise correlations imply strongly correlated network states in a neural population, Nature **440**, 1007 (2006).

[50] C. Giusti, E. Pastalkova, C. Curto, and V. Itskov, Clique topology reveals intrinsic geometric structure in neural correlations, Proceedings of the National Academy of Sciences **112**, 13455 (2015).

[51] L. Merchan and I. Nemenman, On the Sufficiency of Pairwise Interactions in Maximum Entropy Models of Networks, Journal of Statistical Physics **162**, 1294 (2016).

[52] E. Schneidman, S. Still, M. J. Berry, and W. Bialek, Network information and connected correlations, Phys. Rev. Lett. **91**, 238701 (2003).

[53] D. M. Blei, A. Y. Ng, and M. I. Jordan, Latent Dirichlet Allocation, J. Mach. Learn. Res. **3**, 993–1022 (2003).

[54] L. L. Campbell, Exponential entropy as a measure of extent of a distribution, Zeitschrift für Wahrscheinlichkeitstheorie und Verwandte Gebiete **5**, 217 (1966).

[55] T. Cover and J. Thomas, *Elements of Information Theory* (Wiley, 2006).

[56] J.-G. Young, G. Petri, and T. P. Peixoto, Hypergraph reconstruction from network data, Communications Physics **4**, 135 (2021).

[57] R. Mastrandrea, J. Fournet, and A. Barrat, Contact Patterns in a High School: A Comparison between Data Collected Using Wearable Sensors, Contact Diaries and Friendship Surveys, PLOS ONE **10**, 1 (2015).

[58] M. E. J. Newman and A. Clauset, Structure and inference in annotated networks, Nature Communications **7**, 11863 (2016).

[59] M. Contisciani, E. A. Power, and C. De Bacco, Community detection with node attributes in multilayer networks, Scientific Reports **10**, 15736 (2020).

[60] A. Badalyan, N. Ruggeri, and C. De Bacco, Hypergraphs with node attributes: structure and inference, (2023), arXiv:2311.03857 [cs.SI].

[61] N. W. Landry, J.-G. Young, and N. Eikmeier, The simpliciality of higher-order networks (2023), arXiv:2308.13918 [physics.soc-ph].

[62] To deal with large $N_\#$ and κ_d that cannot be stored in memory, we approximate the binomial in Eq. (E2) with a Gaussian

$$\mathcal{N}\left(\frac{\pi_\#}{\kappa_d}N_\#, \frac{\pi_\#}{\kappa_d}N_\#\left(1 - \frac{\pi_\#}{\kappa_d}\right)\right)$$

Crucially, the Gaussian's mean and variance only involve the ratio $N_\#/\kappa_d$, which is numerically stable. We adopt this approximation when the Gaussian's variance exceeds 10.

[63] A Poisson approximation of the binomial

$$\text{Pois}\left(N_\#\frac{\pi_\#}{\kappa_d}\right)$$

is used if $N_\# > 20$ and $N_\#\pi_\#/\kappa_d < 0.1$, or if $N_\# > 100$ and $N_\#\pi_\#/\kappa_d < 10$.

[64] For $n > 5$, we adopt the Ramanujan approximation [66]

$$\log n! \approx n\log n - n\frac{\log\left(\frac{1}{30} + n(1 + 4n(1 + 2n))\right)}{6} + \frac{\log\pi}{2},$$

giving error of order $O\left(1/n^3\right)$.

[65] P. S. Chodrow, Configuration models of random hypergraphs, Journal of Complex Networks **8**, cnaa018 (2020).

[66] S. Ramanujan, *The Lost Notebook and other Unpublished Papers* (Narosa, New Delhi, 1987).